ISBN: 978-3-95450-239-4 ISSN: none doi: 10.18429/JACoW-EBIST2022

Table of Contents

ISBN: 978-3-95450-239-4 ISSN: none doi: 10.18429/JACoW-EBIST2022-WE2WH02

PICOSECOND LASER ABLATION AND ION CLUSTERS FOR EXTERNAL INJECTION INTO THE EXTENDED EBIS*

S. Kondrashev†, E. Beebe, T. Kanesue, M. Okamura,
Brookhaven National Laboratory, Upton, NY 11973, USA
R. Scott, Argonne National Laboratory, Argonne, IL 60439, USA

Abstract

The Extended Electron Beam Ion Source (EBIS) is currently going through final development and offline testing and will replace Relativistic Heavy Ion Collider (RHIC) EBIS as a main ion injector for both RHIC and National Aeronautics and Space Administration (NASA) Space Radiation Laboratory in the beginning of 2023. Due to its longer ion trap, the Extended EBIS will enhance the maximum available beam intensity of Au^{32+}ions by 40 - 50% compared to RHIC EBIS. The inclusion of a high efficiency gas injection module will give Extended EBIS an improved capability to generate intense beams of light ions, such as $^4He^{2+}$ and $^3He^{2+}$. With a further upgrade, the Extended EBIS will also produce polarized $^3He^{2+}$ ions for the future Electron-Ion Collider (EIC). Similarly to RHIC EBIS, charge breeding mode will continue to be important for Extended EBIS. Singly charged ions produced in external ion sources will be accumulated in the Extended EBIS, contained until required charge state is reached, and then extracted from the EBIS in intense pulses of highly charged ions. Two attractive options for external ion sources of singly charged ions which can significantly improve the operational flexibility and stability of Extended EBIS are a picosecond laser ion source and a cluster ion source. A laser with high rep-rate can produce quasi continuous singly charged ion beams from elements of solid targets for periods of tens of milliseconds, making it possible to take advantage of the ability of the EBIS to trap singly charged ions in accumulation injection mode. We studied the properties of different element plasmas generated by a ps-laser with 1.27 mJ energy within an 8 ps pulse to investigate feasibility and specify parameters of a laser ion source for Extended EBIS using both accumulation and single pulse injection modes. It is shown that both injection modes are accessible with a single ion source geometry and single injection line. For most of gaseous elements, a source of cluster ions is quite an attractive option. Cluster ion beams have multiple advantages for external injection into EBIS trap in comparison with atomic ion beams. The electrical current required to deliver the same number of atoms into the trap is several magnitudes lower in both single pulse and accumulation injection modes in this case. It is especially advantageous that even single pulse injection mode for hydrogen and helium clusters with cluster size of about 1000 atoms becomes feasible. It is shown that cluster ion beam with the same particle current is easier to transport and inject into the EBIS trap due to less severe space charge effects. A cluster ion source with the required intensity is viable and can be designed, built, optimized, and tested.

* Work supported by the US Department of Energy under contract number DE-SC0012704 and by the National Aeronautics and Space Administration.
† skondrashev@bnl.gov

EXTENDED EBIS

The Extended EBIS offline testing setup is presented in Fig. 1.

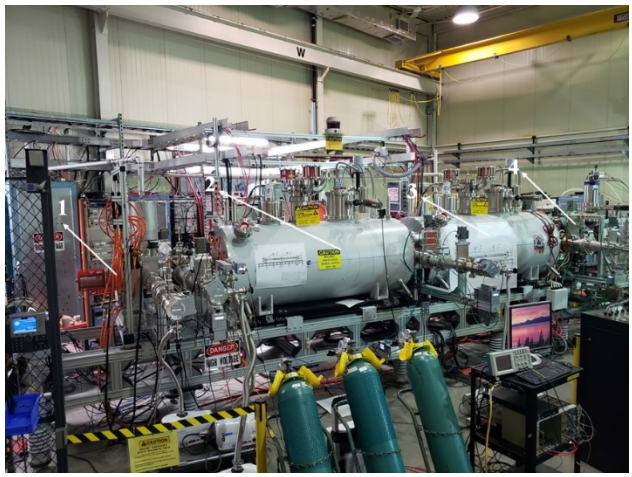

Figure 1: Extended EBIS offline testing setup (1 – electron gun, 2 and 3 – 2 m, 5 T superconducting solenoids, 4 – electron collector).

The main features of Extended EBIS are:

- New oxide electron gun (e-gun) cathode with significantly lower operational temperature compared to previously used IrCe cathode
- Lorenz pulsed gas valve to inject different gasses directly into drift tube structure
- Two custom high capacity ZAO NEG linear modules mounted right in a vicinity of the ion traps [1]
- Advanced vacuum system [2]
- Quadrant electron beam detector for electron beam alignment and measurement of back streaming from the collector electrons placed in between superconducting solenoids [3].

We plan to complete offline testing of Extended EBIS by the end of this summer with following source relocation, installation, and commissioning in the injector area.

"FAST" AND "SLOW" ION INJECTION MODES INTO EBIS

For most of ion species the Extended EBIS will operate as a charge bleeder of 1+ ions injected from external ion sources, although some gaseous species will be injected by

ISBN: 978-3-95450-239-4 ISSN: none doi: 10.18429/JACoW-EBIST2022-WE2WH02

Lorenz pulsed gas valve. Currently for RHIC EBIS (and later for the Extended EBIS), a Laser Ion Source (LIS) provides (and will provide) 1+ ions for most species of solid materials in a high current single pulse ("fast") injection mode [4], and two Hollow Cathode Ion Sources (HCIS) provide 1+ ions of both gaseous and solid species in a lower current accumulation ("slow") injection mode [5].

"Fast" and "slow" external ion injection modes into the EBIS trap are illustrated in Figs. 2 and 3. In the "fast" injection mode, (Fig. 2) the potential of the trap exit barrier is lowered to accept an incoming beam of 1+ ions and then raised to trap the ions after the time for one "round-trip" worth of 1+ ions. In the "fast" mode, efficiencies often more than 50% can be achieved. For the Extended EBIS trap with a length of 2.5 m, the typical "round-trip" time of these ions will be in the range of 100-300 μs for heavy elements of periodic table. In the "slow" injection mode (Fig. 3), the potential of the trap exit barrier is set just below the potential of the external ion source potential. If an injected ion is ionized further by the electron beam before exiting the trap region, it will remain in the trap as it is captured by the potential barrier. The "slow" injection mode efficiency is much lower compared to "fast" injection mode, typically <5%, but in the "slow" mode one can inject and accumulate ions into the EBIS trap for tens of ms which is advantageous in some cases.

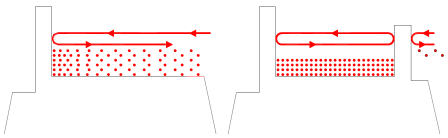

Figure 2: "Fast" ion injection mode into the EBIS trap (the potential of the trap exit barrier is lowered to accept an incoming beam of 1+ ions (left panel) and then raised to trap the ions after the time for one "round-trip" worth of 1+ ions (right panel). Red dots indicate injected 1+ ions and red lines schematically represent their trajectories).

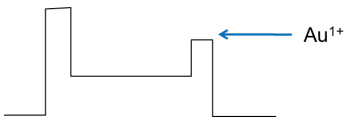

Figure 3: "Slow" ion injection mode into the EBIS trap (energy of injected 1+ ions is just slightly above of the potential of the trap exit barrier, so injected 1+ ions can enter the trap. If an injected ion is ionized further by the electron beam before exiting the trap region, it will not be able to escape past the trap barrier since the applied potential will now be almost twice as high as necessary for trapping the 2+ ion, comparing to the 1+ ion).

Since the Extended EBIS will act as a charge state multiplier, the stability and reliability of the external ion sources is as important as it is for the Extended EBIS itself. There are two attractive options for upgrade of external sources of 1+ ions to improve Extended EBIS operational performance which are under consideration and investigation. Those options are described below.

PICOSECOND LASER ABLATION

Ps-lasers have advantages for generation of low charge state ions compared to ns-lasers because the influence of heat conductivity on a solid target is negligible in the case of ps-laser ablation for laser pulse durations shorter than 10 ps. By using a laser with high rep-rate, it is possible to produce quasi continuous 1+ ion beams for periods up to tens of milliseconds, making it possible to take advantage of the ability of the EBIS to trap 1+ ions in accumulation ("slow") injection mode.

The slow injection mode of beams from laser ion source has following attractive features:

- the required ion beam current is much lower than for "fast" injection mode
- low current ion beams are easier to transport and inject into the EBIS trap because space charge effects are less severe
- the EBIS pulse to pulse variation of highly charged ions can be improved since the ion pulse to pulse variations for the ps-laser plasma are averaged over a long train of ion pulses accepted by the EBIS
- an isotope separator [6] can be placed downstream of laser ion source to select a single isotope ion beam generated from the targets with natural isotope abundance. This allows the EBIS to accumulate and be filled to a higher capacity with the isotope of interest
- laser ablation provides an intensity advantage compared with the HCIS for species such as Zr, which are difficult to sputter.

We studied the properties of Al, Ti, Cu, Nb, and Ta plasmas generated by a ps-laser with 1.27 mJ energy within an 8 ps pulse to investigate feasibility and specify parameters of a laser ion source for RHIC EBIS and Extended EBIS using accumulation ("slow") injection mode.

A 3D model of target irradiation and the diagnostics chamber specifically designed and built for ion yield measurements is shown in Fig. 4.

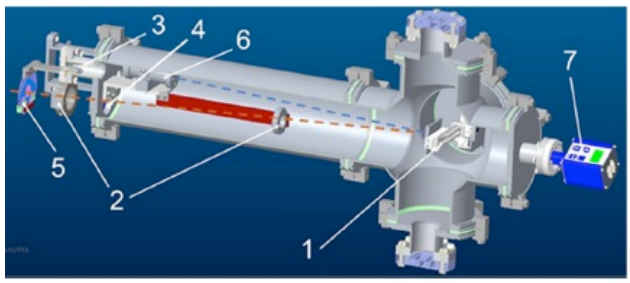

Figure 4: 3D model of the target irradiation and diagnostics chamber: 1—3D target positioner, 2—focusing lens holders, 3—CCD camera, 4—laser input window, 5—fast laser beam shutter, 6—Faraday cup, and 7—vacuum gauge. The laser path is shown by the orange dashed line and the plasma expansion axis is indicated by the blue dashed line.

The laser we used is commercially available from Passat Inc. and has the following parameters: wavelength—1064 nm, pulse width—8 ps, pulse energy—up to 5 mJ/pulse, repetition rate—up to 400 Hz. The maximum average laser pulse energy of this laser at the time of our experiment was

ISBN: 978-3-95450-239-4 ISSN: none doi: 10.18429/JACoW-EBIST2022-WE2WH02

found to be 1.27 mJ with standard deviation 0.06 mJ in a single pulse mode for all measurements described below. A laser beam with diameter of about 10 mm has been focused onto the target surface by lens with 300 mm focal distance mounted inside vacuum chamber. Irradiation angle between laser beam axis and the target normal was equal to 3º. A Faraday cup (FC) with input aperture of 10 mm is placed normally to the target at 57 cm distance and it is equipped with a highly transparent meshed electrode which can be biased up to –1 kV for ion extraction from plasma and for suppression of secondary electrons from the cup. A turbomolecular pump with a 450 l/s pumping speed is attached to the chamber to maintain the residual gas pressure inside the chamber at $2 \cdot 10^{-7}$ Torr. We use 3 ultra-high vacuum, high precision (±50 nm), long travel linear PPS-20 piezo positioner stages (MICRONIX USA) for 3D target positioning. It provides a 51 mm travel range in the horizontal and vertical directions and a 26 mm travel range in the lens focal depth direction. Five metal targets (Al, Ti, Cu, Nb, and Ta), each with dimensions 10 mm by 50 mm, were mounted on the target holder, which was attached to the 3D target positioner.

Parameters of ion yield were measured for both stationary targets and continuously slowly moving targets. The latter option was used to minimize influence of target crater formation on ion yield parameters. Both options are of practical interest for implementation either in "fast" or "slow" ion injection modes into EBIS. Ion current amplitudes, pulse durations (FWHM) and total number of ions registered by FC per single laser shot for all target elements and for stationary and moving targets are summarized in Table 1.

Table 1: Ion current amplitudes (I), pulse durations (FWHM) (Δt) and total number of ions registered by the FC (N) per laser shot for all target elements for both stationary and moving targets with translation speed of 0.05 mm/s

Element		Al	Ti	Cu	Nb	Ta
Stationary target	I, **μA**	48	43	25	37	20
	Δt, **μs**	11.5	15.5	20.4	20.2	42.1
	N	4.8×10^9	5.5×10^9	3.5×10^9	5.8×10^9	6.1×10^9
Moving target	I, **μA**	6	7	4	5	2
	Δt, **μs**	20	30	40	30	60
	N	$\approx 10^9$	$\approx 1.5\times10^9$	$\approx 10^9$	$\approx 10^9$	$\approx 10^9$

All data were obtained using a FC with the 10 mm entrance aperture diameter placed at 57 cm distance from target surface. Numbers for stationary target are taken for fifth laser shot onto the same target spot. All data for moving target are the data for target translation speed of 0.05 mm/s. For the estimation of the number of ions in both cases, it was assumed that most of the ions are singly charged because the laser power density at the target surface is purposely made relatively low. A small fraction of the registered ions could be in higher charge states affecting the accuracy of such estimations.

Detailed description of whole set of experimental results we obtained can be found in [7].

Using data summarized in Table 1, one can specify the main parameters of an ion source which will meet the requirements for external ion injection of singly charged ions into the Extended EBIS. There are scaling equations which are universal for laser ablated plasma dominated by hydrodynamic expansion. These scaling equations were first formulated and applied to laser ion source specification and design in [8] about 25 years ago. If the distance from the target surface to the ion extraction electrode (L) is significantly larger than diameter of extraction electrode aperture (d), and the time-of-flight of ions from target surface to extraction electrode is significantly longer than laser pulse duration, then the ion pulse length (Δt), number of ions (N) and ion current amplitude (I) are scaled with L and d according to following equations [8]:

$$\Delta t \sim L \tag{1}$$

$$N \sim {d^2}/{L^2} \tag{2}$$

$$I \sim {d^2}/{L^3} \tag{3}$$

Once these parameters are measured at a given distance from the target using a given extraction aperture, they can be re-calculated to any distance and extraction aperture diameter using the above scaling equations to achieve the required ion pulse length, number of ions and ion current amplitude.

Detailed description of such specification can be found elsewhere [9]. It was shown [9] that both the "slow" and "fast" injection modes into RHIC EBIS (and Extended EBIS as well) can be provided using a single ps-laser ion source geometry and a single ion injection line, which is the most attractive option for such source of 1+ ions.

Picosecond lasers with 10 kHz rep-rate and with 5 mJ output pulse energy within 6 ps laser pulse became recently commercially available. We have purchased such a laser recently with expected delivery in the end of this year.
After initial experiments to confirm performance of 1+ ion source driven by this ps-laser, we plan to implement such source for external ion injection into the Extended EBIS.

CLUSTER ION SOURCE

Because light ions have relatively high velocity inside EBIS trap, efficient injection of hydrogen and helium ions and filling of the EBIS trap to high capacity is difficult from either LIS or HCIS. To overcome this restriction and

ISBN: 978-3-95450-239-4 ISSN: none doi: 10.18429/JACoW-EBIST2022-WE2WH02

enhance EBIS operational capability we suggest injecting beams of hydrogen and helium cluster ions into EBIS trap.

The challenges of efficient injection of light ions (hydrogen and helium) into EBIS trap both in "slow" and "fast" injection modes are listed below:

- These ions are faster than heavier ions of the same injection energy; therefore, the round-trip time in the trap is shorter and a higher current is required in the "fast" injection mode to inject the required number of ions.
- The charge breeding factor is low (1 or 2), so a high current should be injected in both "fast" and "slow" modes to fully fill the trap
- Transporting a high current ion beam from external source and focusing it into EBIS trap is a challenge due to space charge limitations
- Ionization efficiency in "slow" injection mode is low because most ions exit the trap before being ionized
- Light ions trajectories are influenced more strongly by the magnetic fringe fields of the EBIS solenoids.

All challenges listed above can be mitigated by injection of cluster ions (instead of atomic or diatomic ions) into EBIS trap. Advantages of cluster ion injection into EBIS trap are listed below:

- For the same injection energy trap "round-trip" time is proportional to square route of ion mass. Therefore, ionization probability is higher for clusters in "slow" injection mode and more ions can be injected in "fast" injection mode for the same electric current
- Ionization cross section for clusters is bigger than for atoms which is additional advantage in "slow" injection mode
- A cluster ion beam is easier to inject into EBIS trap because it has low emittance and negligible energy spread due to low temperature of atoms which is required for cluster creation
- Considering clusters with about 1000 atoms size, about 1000 times lower electric current is required to deliver the same number of atoms into the trap. It means that influence of space charge will be much less pronounced during transportation and focusing of cluster ion beam into the trap
- "Fast" injection mode with hydrogen and helium cluster injection becomes feasible as the required electrical current drop proportionally to $M^{-1.5}$ (M is cluster mass)

Clusters of all sizes (masses) will be transported and injected into the trap because all injection lines for the Extended EBIS are electrostatic.

Let's compare required electric currents for atomic and cluster ion beam injection into the Extended EBIS. The electric currents required to fully fill the Extended EBIS trap are estimated below for both the "fast" and "slow' injection modes, for singly charged atomic and cluster ions.

In "fast" injection mode, the required electric current of singly charged clusters with n atoms of element E in cluster is defined by following equation:

$$I_{E_n^+} = \frac{Q}{t \cdot k \cdot n \cdot \alpha} \tag{4}$$

where Q is trap capacity (in Coulombs), t is trap "round-trip" time, $k = z$ is breeding factor (z is the mean charge state in the end of breeding cycle), α is trapping efficiency.

Considering that:

$$t = \frac{2 \cdot L}{V} \tag{5}$$

$$V = \sqrt{\frac{2 \cdot E_{inj}}{n \cdot m}} \tag{6}$$

where L is trap length, V is ion velocity in the trap, E_{inj} is injection energy of ions, m is atomic mass of element E, one can find that:

$$I_{E_n^+} = \frac{Q \cdot \sqrt{E_{inj}}}{L \cdot k \cdot n^{3/2} \cdot \alpha \cdot \sqrt{2 \cdot m}} \tag{7}$$

As one can see from equation (7) that required current drops significantly with increasing cluster size n.

An injection energy of about half of the Extended EBIS electron beam depth in the trap (≈ 750 eV) is needed for helium ions to fully (more accurately almost fully) fill the trap considering that trapping efficiency α is about 100% for atomic ions. Using these numbers for equation (4) one can find that electric current of helium ions $I_{He_1^+}$ required to fully fill RHIC EBIS trap is about 3.4 mA. The electric current of helium cluster ions with 1000 atoms in cluster $I_{He_{1000}^+}$ is about 1.1 μA considering the same injection energy of 750 eV and conservatively trapping efficiency α of about 10%. Based on space charge estimations below it will be shown that there is significant advantage in transporting and focusing of cluster ion beams compared to atomic ion beam for this ratio of electric currents.

In the "slow" injection mode electric current of singly charged clusters with n atoms of element E in cluster required to fully fill trap is defined by following equation:

$$I_{E_n^+} = \frac{Q}{\Delta t_{inj} \cdot \beta \cdot n} \tag{8}$$

where Δt_{inj} is duration of ion injection and β is ionization efficiency within trap "round-trip".

Taking for estimations $\Delta t_{inj} \approx 20$ ms and $\beta \approx 1\%$ one can find that required electric current is about 800 μA and 800 nA in the case of atomic and cluster ion injection correspondently. One should mention that ionization efficiency for cluster ion injection can be higher because cluster ions are slower and spend more time in the trap. Ionization cross section is also higher for cluster ions compared to atomic ions. These two factors can further enhance advantages of cluster ion injection into EBIS trap in "slow" injection mode. There is significant uncertainty here concerning how clusters will be disintegrated inside electron beam and what would be their trapping efficiency by electron beam space charge. It depends mainly on ion (or atom) transverse energy gained because of electron-cluster collision. We were not able to find clear answer to this question in literature.

Over the last 20 years significant progress has been made in the development of intense sources of cluster ions and generation of gas cluster ion beams with average size of

ISBN: 978-3-95450-239-4 ISSN: none doi: 10.18429/JACoW-EBIST2022-WE2WH02

few thousand atoms per cluster and 1 μA electrical current has been demonstrated for material applications [10, 11]. Cluster ion beams with such parameters are well suited for both "fast" and "slow" injection modes into EBIS trap.

The influence of space charge on ion beam transport (and focus) for cluster and atomic ions is compared using following equations. The divergence of an initially parallel beam is defined by [12]:

$$r(z) \approx r(z=0) \cdot (1 + 0.5 \cdot K \cdot (\frac{z}{r_0})^2) \qquad (9)$$

where $r(z)$ is beam radius at coordinate z, r_0 - beam radius at z = 0 (beam is parallel there) and K is generalized perveance.

Generalized perveance can be found from the following expression:

$$K = \frac{I}{V^{3/2}} \cdot [\frac{1}{4\pi\varepsilon_0 (2q/M)^{1/2}}] \qquad (10)$$

where I is electrical beam current, V is source extraction voltage, q and M are ion charge state and mass and ε_0 is vacuum permittivity.

As one can see generalized perveance is proportional to the square root of the ion mass for the same electrical beam current:

$$K \propto I \cdot M^{1/2} \qquad (11)$$

Considering that the required electrical current I_M for cluster beam with mass M (N atoms in cluster) to transport the same particle current as atomic ion beam (I_1) is equal to:

$$I_M = \frac{I_1}{N} \propto \frac{I_1}{M} \qquad (12)$$

Then, one can find that generalized perveance for cluster beam with mass M and required electrical current I_M is defined by:

$$K_M \propto I_M \cdot M^{1/2} \propto \frac{I_1}{M^{1/2}} \qquad (13)$$

Based on equation (13), one can conclude that there is significant advantage to transport (and focus) cluster ion beams compared to atomic ion beams with the same particle current because space charge effects are inversely proportional to square root of the ion mass.

CONCLUSION

The Extended EBIS is under the final testing and will replace RHIC EBIS as a main ion injector for RHIC and NSRL in the beginning of 2023. There are two attractive options for upgrade of external sources of 1+ ions to improve operational performance of the Extended EBIS which are under consideration and investigation.

One option is the laser ion source based on ps-laser. To evaluate feasibility of such ion source, we have measured ion beam current amplitudes and pulse durations (FWHM) for different target elements with both stationary and moving targets. Using these data along with laser ablated plasma scaling equations, the geometry of a ps-laser-based ion source which will meet requirements for external ion injection into the Extended EBIS trap in both the ''fast'' and ''slow'' injection modes has been specified. It is shown that both ''slow'' and ''fast'' injection modes can be accommodated with a single ion source geometry and within single injection line.

Another option is a cluster ion source. Cluster ion beams have multiple advantages for external injection into EBIS trap in comparison with atomic ion beams. The electric current required to deliver the same number of atoms into the trap is several magnitudes lower in both "fast" and "slow" injection modes for clusters. It is especially attractive that the "fast" injection mode for hydrogen and helium clusters with cluster size of about 1000 atoms becomes feasible, whereas for molecular or atomic injection the slow mode was necessary to achieve reasonable accumulation of ion charge. It is shown that cluster ion beam with the same particle current is much easier to transport and focus into the trap due to much lower space charge repulsion.

REFERENCES

[1] S. Kondrashev *et al*., "Development of highly efficient NEG pumping system for EBIS", *Review of Scientific Instruments* 90 (11), 113307, 2019. doi:10.1063/1.5127751

[2] S. A. Kondrashev *et al.*, "Development of a Compact Linear ZAO NEG Pumping System", in *Proc. ECRIS'20*, East Lansing, MI, USA, Sep. 2020, pp. 167-171. doi:10.18429/JACoW-ECRIS2020-NACB01

[3] S. Ikeda *et al.*, "Double-sided detector for electron beam alignment and measurement of back-streaming electrons in Extended EBIS at BNL", *J. Phys.: Conf. Ser.* 2244 012085, 2022. doi:10.1088/1742-6596/2244/1/012085

[4] T. Kanesue *et al.*, "The commissioning of the laser ion source for RHIC-EBIS" in *Proc. Int. Particle Accelerator Conf. (IPAC'14)*, Dresden, Germany, WEOAB01, 2014.

[5] J. Alessi *et al.*, "A hollow cathode ion source for production of primary ions for the BNL electron beam ion source", *Review of Scientific Instruments* 85, 02C107, 2014.

[6] S. Kondrashev *et al.*, "Isotope separator for external ion injection into EBIS", *AIP Conference Proceedings* 2011, 080005, 2018. doi: 10.1063/1.5053360

[7] S. Kondrashev *et al.*, "Features of ion generation by a picosecond laser in the range of $10^{11} – 10^{13}$ W/cm−2 power densities", *Plasma Res. Express* 3, 045002, 2021.

[8] B. Yu. Sharkov and S.A. Kondrashev, "Matching of the intensive laser ion source to the RFQ accelerators", in *Proc. European Particle Accelerator Conf. (EPAC'1996),* Barcelona, Spain, p 1550, 1996.

[9] S. Kondrashev *et al.*, "Picosecond laser generated plasma as a source of singly charged ions for external injection into an EBIS", *Nuclear Inst. and Methods in Physics Research, A* 1010, 165563, 2021.

[10] I. Yamada, "Historical milestones and future prospects of cluster ion beam technology", *Applied Surface Science* 310, 2014, 77-88.

[11] https://xpssimplified.com

[12] M. Reiser, "Theory and design of charged particle beams" (second edition), 2008.

ISBN: 978-3-95450-239-4 ISSN: none doi: 10.18429/JACoW-EBIST2022-WE3WH03

THE JENA S-EBIT FACILITY

T. Morgenroth[1,2 *], S. Trotsenko, S. Bernitt[1,2],
GSI Helmholtzzentrum für Schwerionenforschung GmbH, Darmstadt, Germany
G. Vorobyev, GSI Helmholtzzentrum für Schwerionenforschung GmbH, Darmstadt, Germany
R. Schuch[1], Stockholm University, Stockholm, Sweden
Th. Stöhlker[2,3], Helmholtz Institute Jena, Jena, Germany
[1]Helmholtz Institute Jena, Jena, Germany
[2]IOQ Friedrich-Schiller-University Jena, Jena, Germany
[3]GSI Helmholtzzentrum für Schwerionenforschung GmbH, Darmstadt, Germany

Abstract

Electron beam ion traps (EBITs) are versatile tools for spectroscopic studies of partially ionized atomic systems, mainly in the x-ray domain. This yields valuable information for fundamental atomic physics as well as astrophysics. Ion charge state distributions, resulting from ionization and recombination processes, can be observed and used to benchmark plasma dynamics. Furthermore, EBITs can be used as small stand-alone ion sources, as they are already used for example at the HITRAP facility. The Jena S-EBIT facility are two EBITs, the former R- and S-EBIT from Stockholm, which both are suitable for x-ray spectroscopy studies and ion extraction. S-EBIT I has been used as a tool for x-ray spectroscopy, including the testing of newly developed x-ray detectors, like the magnetic metallic micro-calorimeter maXs30. In addition, the setup was expanded by a testing beamline, to evaluate the potential of S-EBIT I as an ion source. S-EBIT II is currently in commissioning for operation as a standalone ion source for HITRAP in the near future. This will provide new opportunities for local experiments, like the ARTEMIS experiment, independently from the Gesellschaft für Schwerionenforschung (GSI) accelerator infrastructure.

INTRODUCTION

The two Jena S-EBIT traps are based on the cryogenic R- and S-EBIT from the AlbaNova University Centre in Stockholm. R-EBIT was set up in 2005 and used for x-ray studies and measurements with extracted and charge-separated ions. The construction of the S-EBIT upgrade started in 2008, with the aim to increase the maximum electron-beam energy from 30 to 260 keV [1]. In 2013/14 all R- and S-EBIT parts were moved to the GSI Helmholtzzentrum für Schwerionenforschung in Darmstadt. Here, they were assembled as two independent EBITs, S-EBIT I & II. While S-EBIT I is already in operation, S-EBIT II is currently in commissioning.

THE FACILITY

The design of both EBITs is based on the Super EBIT from the Lawrence Livermore National Laboratory [2], with a difference that cooling of the super conducting magnet of each EBIT is achieved by means of a cold head and therefore both setups are liquid helium free. The operating parameters of both EBITs are listed in Table 1.

Table 1: S-EBIT Operating Parameters Comparison

Parameter	S-EBIT I	S-EBIT II
Type	Cryogenic (liquid helium free)	
Magnetic field	3 T	4 T
Electron-beam energy	40 keV	260 keV
Electron-beam current	180 mA	250 mA
Electron-beam radius (80%)	37 µm	
Trap length	2 cm	
Ions per pulse	10^7	
Maximum charge state	U^{72+}	U^{92+}
Status	Operating	Commissioning

S-EBIT I

S-EBIT I is at the moment in operation as part of the Jena S-EBIT facility. It is used as tool for x-ray spectroscopy studies, with electron-beam energies of up to 40 keV. This is realised by having the drifttubes operating at positive high voltages while the cathode is kept at ground potential. A section view of the setup is shown in Figure 1.

S-EBIT I is a reliable x-ray source, providing fluorescence from several different ion species, including heavy highly charged ions. This enables the ability of testing newly de-

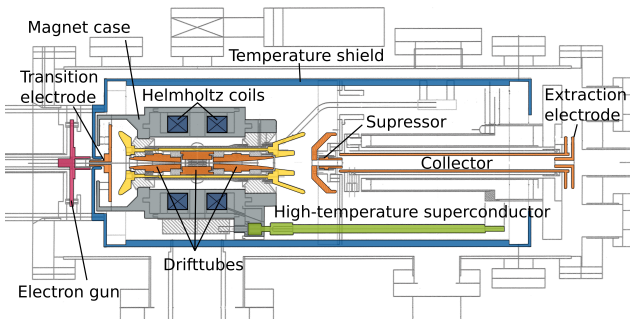

Figure 1: Technical sketch of S-EBIT I.

* t.morgenroth@hi-jena.gsi.de

ISBN: 978-3-95450-239-4 ISSN: none doi: 10.18429/JACoW-EBIST2022-WE3WH03

veloped detector systems, as well as commission them in a realistic environment for their intended use, by performing real measurements.

This has been done to prepare the metallic, magnetic calorimeter maXs30 for a beam time at the storage ring CRYRING@ESR. This commissioning run was finished successfully, and showed the great potential of the maXs30 detector, as illustrated in the x-ray spectrum in Figure 2, in which Kα transitions of different charge states of iron are spectrally resolved [3].

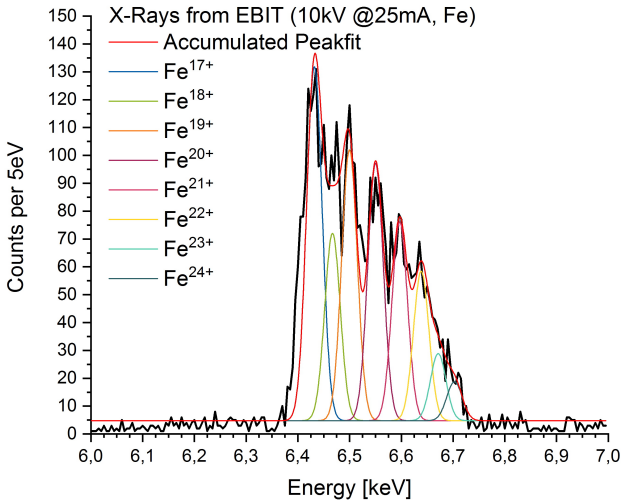

Figure 2: Measured x-ray spectra with the maXs30 detector.

Furthermore, to evaluate S-EBIT I as a potential ion source, it has been equipped with a testing beamline, including multiple faraday cups, ion optics and a 90° bending magnet. First measurements are planned to be conducted until the end of this year.

S-EBIT II

S-EBIT II is currently in commissioning and will be used as a local ion injector for the HITRAP facility in the near future.

The HITRAP facility decelerates, captures and cools heavy, highly charged ions provided by the GSI accelerator infrastructure. To that end it is directly connected to the experimental storage ring (ESR) [4]. Cooled ion packages can be provided to experiments at HITRAP, like the ARTEMIS g-factor or the SPECTRAP experiment [5,6]. As the need for ions at HITRAP is higher than what the GSI accelerator infrastructure can provide, local ion sources play an important role to close this gap. EBITs are well suited for this task, as they are able to produce high-intensity ion beams of well-defined ion species and charge states. The HITRAP facility is already using the compact SPARC EBIT as a local injector. The addition of S-EBIT II as local injector for HITRAP aims to extend the field of ions species that can be used, even when HITRAP does not receive ions from the GSI accelerator infrastructure [7].

A picture of S-EBIT II is shown in Figure 3. The drift tube structure is identical to that of S-EBIT I. The difference

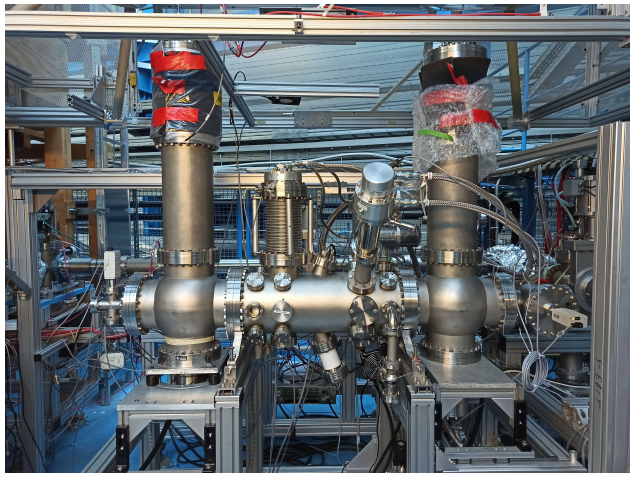

Figure 3: Picture of S-EBIT II. The electron gun is in the left tower and the collector in the right tower. Ions will be extracted to the right.

to S-EBIT I is, that for S-EBIT II the electron gun and the collector are operating on a high, negative potential of up to -220 kV. To be able to focus electron beams of those higher energies, S-EBIT II is equipped with a stronger superconducting magnet, which can be powered up to a magnetic field of 4 T at trap center.

In the ongoing commissioning, the cryogenic system, together with the superconducting magnet was already successfully tested, with the magnet being in stable operation at 4 T. The upgraded high-voltage system is almost completed and has been partially tested, with only the new power supply for the drifttubes still missing. It is expected to be delivered, installed and tested until August 2022. The electron gun is currently in commissioning. Within the next months, the initial commissioning will be completed, with the EBIT running at an electron-beam energy of up to 20 keV. In this limited mode, S-EBIT II gun, collector and trap will be running at potentials of ±10 kV. In the medium term, we plan to use the EBIT with electron-beam energies of up to 140 keV, with -100 kV at the gun and collector and +40 kV at the trap.

CONCLUSION

The Jena S-EBIT facility is a valuable support for various experiments. Besides providing the possibility for spectroscopy studies of highly charged ions in confined plasmas by itself, it can serve as a tool for commission and testing of newly developed x-ray detectors, like micro-calorimeters. Additionally, it can be used as an ‘offline’ ion source for heavy, highly charged ions at a high availability in comparison to storage rings.

REFERENCES

[1] Schuch, Reinhold, Stanislav Tashenov, Istvan Orban, Matthias Hobein, Sultan Mahmood, O. Kamalou, Nadeem Akram et al. "The new Stockholm Electron Beam Ion Trap (S-EBIT)." *Journal of Instrumentation* 5, no. 12 (2010): C12018.

ISBN: 978-3-95450-239-4 ISSN: none doi: 10.18429/JACoW-EBIST2022-WE3WH03

[2] Knapp, D. A., R. E. Marrs, S. R. Elliott, E. W. Magee, and R. Zasadzinski. "A high-energy electron beam ion trap for production of high-charge high-Z ions." *Nuclear Instruments and Methods in Physics Research Section A: Accelerators, Spectrometers, Detectors and Associated Equipment* 334, no. 2-3 (1993): 305-312.

[3] Herdrich, Marc O., Andreas Fleischmann, Daniel Hengstler, Steffen Allgeier, Christian Enss, Sergiy Trotsenko, Tino Morgenroth, Reinhold Schuch, Günter Weber, and Thomas Stöhlker. "High-precision X-ray spectroscopy of Fe ions in an EBIT using a micro-calorimeter detector: First results." *X-Ray Spectrometry* 49, no. 1 (2020): 184-187.

[4] Kluge, H-J., T. Beier, K. Blaum, L. Dahl, S. Eliseev, F. Herfurth, B. Hofmann et al. "HITRAP: a facility at GSI for highly charged ions." *Advances in Quantum Chemistry* 53 (2008): 83-98.

[5] Vogel, Manuel, Mohammad Sadegh Ebrahimi, Zhexi Guo, Anahita Khodaparast, Gerhard Birkl, and Wolfgang Quint. "Electron magnetic moment in highly charged ions: The ARTEMIS experiment." *Annalen der Physik* 531, no. 5 (2019): 1800211.

[6] Murböck, Tobias, Sebastian Albrecht, Zoran Andelkovic, Radu Cazan, Volker Hannen, Raphael Jöhren, Jonas Vollbrecht et al. "SpecTrap: precision spectroscopy of highly charged ions—status and prospects." *Physica Scripta* 2013, no. T156 (2013): 014096.

[7] Andelkovic, Z., F. Herfurth, N. Kotovskiy, K. König, B. Maaß, T. Murböck, D. Neidherr et al. "Beamline for low-energy transport of highly charged ions at HITRAP." *Nuclear Instruments and Methods in Physics Research Section A: Accelerators, Spectrometers, Detectors and Associated Equipment* 795 (2015): 109-114.

ISBN: 978-3-95450-239-4 ISSN: none doi: 10.18429/JACoW-EBIST2022-WE4WH03

NUCLEAR DECAY STUDIES OF HIGHLY CHARGED RADIOACTIVE IONS AT TITAN

J. Ash*, Z. Hockenbery, J. Ringuette, A. Kwiatkowski, I. Dillman, A. Lennarz
TRIUMF, 4004 Wesbrook Mall, Vancouver, BC, Canada V6T 2A3
K. Leach, Colorado School of Mines, Golden, CO, USA
L. Brunner, McGill University, Montreal, QC, Canada

Abstract

Interactions between the atomic nucleus and its surrounding electrons can have a large impact on the decay modes of rare-isotopes. Partial or complete ionization of radioactive nuclei can open new exotic decay modes, such as nuclear excitation via electron capture, or selectively block decay modes to expose second order processes, such as double-gamma decay. The TITAN Electron Beam Ion Trap (EBIT) at TRIUMF has successfully been used to generate and store highly charged radioactive ions, while also providing a controlled, low-background environment for decay spectroscopy.

INTRODUCTION

When investigating the decay of radioactive nuclei, interactions between the nucleus and bound electrons in the constituent atom are typically ignored. However, in common modes of electroweak decay such as electron capture and internal conversion, the probability of decay is significantly affected by the spatial distribution of the atom's electron cloud. For nuclear beta decay, the energy and momentum distributions of the emitted positron or electron are modified by the surrounding orbital electrons. Understanding the nature of these decay modes requires not only knowledge of the nuclear structure of the initial and final states, but also the effects of the atomic charge state on the decay itself.

Studies of the electroweak decay modes of highly charged ions (HCIs) offer an experimental challenge due to the significant technical obstacles of creating and storing radioactive nuclei at high charge states. The Experimental Storage Ring at GSI in Darmstadt, Germany, has been used to study the effects of charge state on electron capture [1] for over 30 years. The work presented in this article represents the only other attempt to study radioactive HCI decays, and the world's only low-energy ion trap decay station.

DECAY SPECTROSCOPY WITH THE TITAN EBIT

The Isotope Separator and Accelerator (ISAC) [2] facility at TRIUMF in Vancouver, Canada, provides a broad array of rare-isotope beams (RIBs) using the isotope separation online (ISOL) technique [3]. The TRIUMF cyclotron produces a 500-MeV proton beam at up to 100 µA. The high-intensity proton beam impinges on a production target, yielding radioactive ions from spallation and fission reactions. The RIB of interest is separated according to mass to charge ratio and delivered to one of TRIUMF's experimental facilities.

TRIUMF's Ion Trap for Atomic and Nuclear Science (TITAN) utilizes multiple traps and instruments in conjunction to study short-lived nuclei [4]. As shown in Figure 1, a radio-frequency quadrupole (RFQ) linear Paul trap is used for cooling via buffer gas and bunching the single-charge ion (SCI) beam. The Measurement Penning Trap (MPET) and Multi-reflection Time of Flight Mass Spectrometer (MR-TOF-MS) are primarily used for precision mass measurements. Lastly, the Electron Beam Ion Trap (EBIT) generates and traps HCIs, both for delivery to the MPET and for decay spectroscopy.

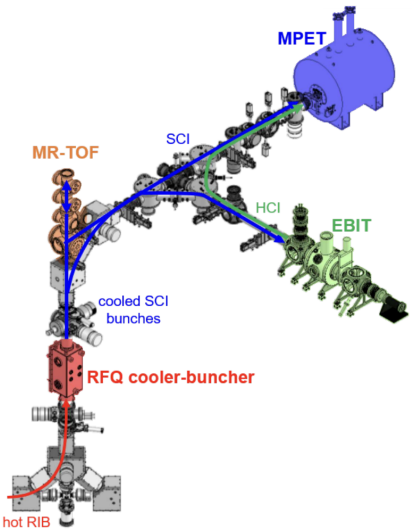

Figure 1: A diagram of the TITAN facility. The ISAC beam (red) is injected into the RFQ cooler-buncher, and the resulting singly-charged ion beam (blue) is delivered to one of several ion traps that comprise TITAN. In the Electron Beam Ion Trap (EBIT), ions are charge bred to higher charge states and either sent to the Measurement Penning Trap (MPET) or trapped in the EBIT for decay spectroscopy, as in this work.

After successfully being used for the charge breeding of stable ions at the Max-Planck-Institut für Kernphysik in Heidelberg, Germany, the FLASH-EBIT design was repurposed for RIBs at TRIUMF in the form of the TITAN EBIT (Figure 2) [5]. Axial confinement in the trap itself is provided by an electrostatic quadrupole potential well created by nine copper drift tubes. The drift tubes are held at specific voltages to create the potential profile of the trap, which is

* jash@triumf.ca

ISBN: 978-3-95450-239-4 ISSN: none doi: 10.18429/JACoW-EBIST2022-WE4WH03

modified in cycles to stack new SCIs into the trap as well as extract HCIs for mass measurements. Radially, ions are confined by superconducting magnets in a Helmholtz configuration around the trap center, and the negative space charge of the incoming beam of electrons. The two superconducting magnets generate a magnetic field of up to 6 Tesla and are thermally coupled to the copper drift tubes. Formerly, the cathode in the electron gun of the TITAN EBIT was capable of producing 500 mA, 2keV electron beams, resulting in 10^9 electrons in the trapping region [6]. Recently, upgrades have been planned which will potentially improve the current density, and thus the strength of confinement, caused by the electron space charge.

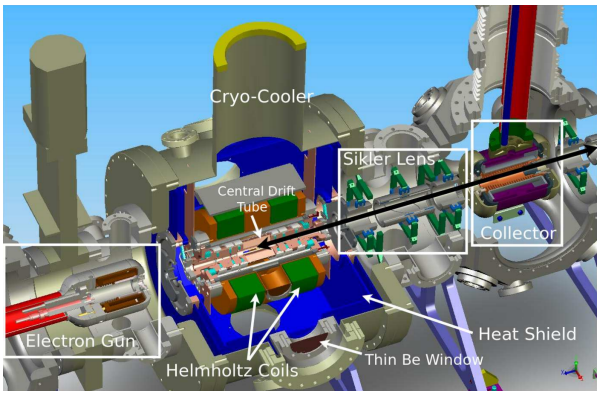

Figure 2: Design of the TITAN EBIT [7]. Beam travels along the black arrow into the trap and interacts with the electron beam via electron impact ionization. Electrostatic potential from the drift tubes, in combination with superconducting magnets and the negative space charge of the electron beam, confine ions for charge breeding, followed by decay or ejection from the trap.

The TITAN EBIT was commissioned for two purposes: providing HCIs to improve the precision of mass measurements [5, 8], and to provide a unique environment for the study of exotic nuclear decay modes [9]. The latter case is facilitated by the direct access to the trap center afforded by seven external ports perpendicular to the EBIT axis (see Figure 3). The seven ports are spaced at 45° at slightly different distances, as shown. These ports are separated from the vacuum of the trap (roughly 10^{-11} Torr) by 0.25 mm-thick beryllium windows. The beryllium windows ensure vacuum and thermal isolation of the trap, while minimizing attenuation of gamma and X-rays produced from nuclear and atomic decays. Several different detectors and arrays have been used at the TITAN EBIT, including five to seven lithium-drifted silicon (Si(Li)) detectors [10]. More recently, an array of High-Purity Germanium (HPGe) detectors has been proposed, consisting of detectors formerly used in the 8π array [11]. The decision to change to HPGe detectors was in part due to their greater efficiency at high gamma-ray energies without sacrificing resolution, which can counteract the relatively low angular coverage of the EBIT setup compared to more traditional decay-station experiments.

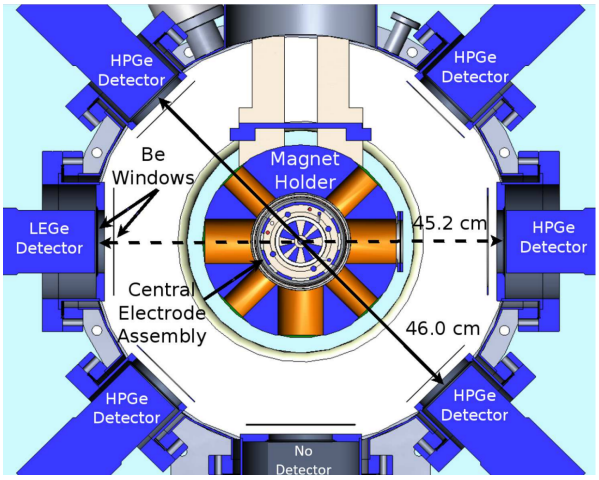

Figure 3: Cross-sectional view of the TITAN EBIT with six of the seven external ports in use.

UPCOMING EXPERIMENTS PROBING RARE NUCLEAR DECAY MODES

The TITAN EBIT is uniquely capable of providing a controlled environment to observe exotic nuclear decay modes dependent on atomic charge states. This proceeding presents the physics goals and experimental details for two upcoming experiments at the TITAN EBIT which seek to observe exotic decay modes with gamma-ray spectroscopy.

Nuclear Excitation via Electron Capture

Nuclear Excitation via Electron Capture (NEEC) is the proposed reversed process of the more familiar internal conversion. If a highly charged ion captures an electron into one of its open lower orbitals, there is an excess of energy between the initial kinetic energy of the electron and its final binding energy in the ion. NEEC is said to occur when the energy of an excited nuclear state matches this resonance energy. The nucleus, excited by atomic electron capture, then decays normally, typically with the release of gamma rays. This precise resonance effect is highly selective, a nuclear analogue to the atomic phenomenon of direct recombination. The underlying electron-nucleus interaction occurs by either the Coulomb interaction or virtual photon exchange between the electronic and nuclear currents [12]. While the process has proven to be very difficult to observe experimentally, a theoretical formalism for the calculation of transition rates and cross sections has been developed [13].

The advancement in theory of calculating more advanced internal conversion coefficients and higher predicted NEEC cross sections spurred renewed experimental interest, producing the first claimed observation of NEEC [14]. The experimenters claimed to indirectly observe NEEC events by populating an isomeric state in ^{93m}Mo via fusion-evaporation and measuring the subsequent gamma-ray decays to the ^{93}Mo ground state. NEEC events would be triggered after the ions were fully stripped and implanted in the lead stopping target by the abundant free electrons. The sub-

ISBN: 978-3-95450-239-4 ISSN: none doi: 10.18429/JACoW-EBIST2022-WE4WH03

sequent gamma-ray decays would not occur promptly unless the ^{93m}Mo was excited by some nuclear process, and NEEC is a potential explanation, thus the experimental probability was calculated to be $P_{exc} = 0.010(3)$. Statistical uncertainties in the number of ^{93m}Mo isomers present, the number of free electrons at the NEEC resonant energy, and charge state dependence dominate. However, subsequent theoretical calculations performed for the specific experimental conditions of the ^{93m}Mo NEEC experiment established a best case scenario of $P_{exc} = 5 \times 10^{-11}$, nine orders of magnitude smaller [15]. The disagreement remains unresolved; however, the authors of Ref. [15] indicate that, while not fully accounting for the observed isomeric depletion, Coulomb excitation and inelastic scattering probabilities are predicted to be many orders of magnitude more likely than that of NEEC.

The controlled environment of the TITAN EBIT provides the capacity for a low-background, direct observation of the nuclear decay of HCIs. By precisely tuning the electron beam energy to the NEEC resonance energy, triggering NEEC can occur directly at low energies, with less ambiguity than the previous observation. Once demonstrated, NEEC triggering could open a new and powerful method of selectively populating isomeric states that are challenging to observe otherwise, as well as provide results that improve the existing theoretical framework for the NEEC process. To achieve these goals, an experiment has been approved to probe the NEEC cross section in ^{129m}Sb (see Figure 4). The isomeric $(19/2^-)$ state at 1851 keV can be stimulated via electron capture to excite to the short-lived $(15/2^-)$ state at 1861 keV. This state typically decays via internal conversion, as one would expect for a likely NEEC candidate. However, there is a 10% branching ratio to decay via gamma-ray emission, and detection of the resulting gamma rays are a clear signature of NEEC events. The high energy 1161 keV gamma ray is in a particularly clean region of the EBIT background spectrum for the HPGe array used for this experiment, and will be used for constraining the NEEC cross section. Detailed simulations and theoretical calculations of NEEC cross sections will be included in Ref. [16].

Double-Gamma Decay

The prediction of double-gamma decay is a fundamental result from quantum electrodynamics, which allows for quantum systems in excited states to decay by the simultaneous emission of two photons. As opposed to the ubiquitous single-gamma decay, double-gamma decay is a second-order process in which the sum of the two emitted photon energies are equal to the transition energy ω_0, i.e. the difference in binding energy of the initial and final states. These second order decays have been observed extensively in atomic physics; however, double-gamma decay of excited nuclear states has only been observed in a few special cases [17–20]. The presence of single-gamma decay events dominating over second-order processes make measuring the double-gamma decay contribution experimentally unfeasible. Decays of the form $0^+ \rightarrow 0^+$ to the nuclear

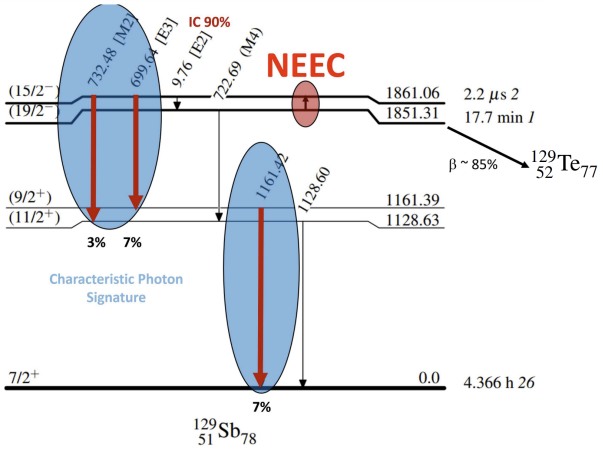

Figure 4: Partial level scheme for ^{129}Sb, showing the characteristic gamma-ray emissions observable after NEEC from the 1851 keV state to the 1861 keV state, along with branching ratios.

ground state are ideal candidates, since $E0$ photon emission is forbidden. If there are no intermediate states available, these states must decay by either double-gamma decay, internal conversion, or internal pair creation. Investigation of these so-called non-competitive double-gamma decay candidates have led to measurements of double-gamma decay for ^{16}O [17], ^{40}Ca [18], and ^{90}Zr [18, 19]. These stable, spherical nuclei with magic numbers of protons and neutrons ($Z = 40$ being a major sub-shell closure) were all shown to have very similar double-gamma decay branching ratios ($\Gamma_{2\gamma}/\Gamma_{total} = 6.6 \times 10^{-4}, 4.5 \times 10^{-4}, 2.2 \times 10^{-4}$ respectively). Moreover, angular correlations between the two gamma rays indicated interference between the $2E2$ and $2M1$ decay modes, which surprisingly were found to have similar order [21].

$$\Gamma_{2\gamma} = \frac{\omega_0^7}{105\pi}\left(\alpha_{E1}^2 + \chi_{M1}^2 + \frac{\omega_0^4}{4752}\alpha_{E2}^2\right) \qquad (1)$$

Equation 1 is an approximation of the decay width for double-gamma decay, where ω_0 is the transition energy, α_{E1} and α_{E1} the electric dipole and quadrupole transition polarizabilities, and χ_{M1} is the magnetic dipole transition susceptibility. The observed double-gamma decay rates are consistent with this approximation, since they are roughly proportional to ω_0^7 ($\Gamma_{2\gamma}/\omega_0^7 \approx 35 \pm 4$ s^{-1} MeV^{-7}). These electromagnetic quantities are sensitive to the nuclear structure properties in the initial and final states, and the strength of decays between these 0^+ states have been linked to coexisting shapes [22]. Therefore, new observations of double-gamma decay in nuclei which exhibit shape coexistence can effectively probe electric and magnetic properties of these nuclei.

Of the six remaining nuclei with known and viable $0_2^+ \rightarrow 0_1^+$ transitions for double-gamma decay measurements, ^{98}Zr is an intriguing case. The nucleus exists at a nuclear shape-phase transition from spherical to deformed ground states

ISBN: 978-3-95450-239-4 ISSN: none doi: 10.18429/JACoW-EBIST2022-WE4WH03

along the Zr isotopic chain [23], though the intensity of the configuration mixing present in ^{98}Zr is not well known. Measurement of the double-gamma decay angular correlations could shed light on this structural evolution. A similar case exists in ^{98}Mo, and an upper limit on the double-gamma decay rate has been established [20].

Despite the name, non-competitive double-gamma decay still competes with internal pair creation and internal conversion as dominant decay modes. In the case of ^{98}Zr, the low transition energy of $\omega_0 = 0.854$ MeV prevents competition with internal pair creation. Internal conversion, however, can only be suppressed if the ion is fully stripped of its atomic electrons. TITAN EBIT's capabilities as an electron beam ion trap are able to provide an environment that removes all competition with the double-gamma decay of ^{98}Zr, as well as furnishing the means of measuring the resulting gamma rays and their angular correlations.

In the approved experiment, a TRIUMF-ISAC primary beam of ^{98}Sr will enter the trap and undergo beta decay, populating the 0_2^+ state in ^{98}Zr (via subsequent ^{98}Y beta decay) with a 15% branching ratio. It has been demonstrated recently that the TITAN EBIT is capable of retrapping beta-decay products [24], which is essential to the experiment. Once the isomeric 0_2^+ state in ^{98}Zr is populated, it is fully ionized to prevent internal conversion. The subsequent two gamma rays are detected in the HPGe array, with yields present in the summed energy spectra at $\omega_0 = 0.854$ MeV (FWHM = 2.7 keV). Based on a primary beam intensity of 1×10^7 pps and a 60-keV electron beam with a current density of $j = 2800$ A/cm^2, measured coincidence yields are estimated at 250 counts per hour of beamtime. Background from beam contaminants and other gamma rays in the full beta-decay chain have been assessed using GEANT4 simulations, to be presented at a later date.

CONCLUSIONS

In summary, decay spectroscopy of radioactive HCIs using the TITAN EBIT provides a unique opportunity to study rare nuclear decay processes. Two cases corresponding to approved experiments at TRIUMF have been presented: NEEC decay of the $19/2^-$ state of ^{129m}Sb, and double-gamma decay of the 0^+ state of ^{98}Zr. These experiments are planned for later this year.

REFERENCES

[1] Y. A. Litvinov and F. Bosch, "Beta decay of highly charged ions," *Reports on Progress in Physics*, vol. 74, no. 1, p. 016 301, Dec. 2010.

[2] P. Bricault, M. Dombsky, P. Schmor, and G. Stanford, "Radioactive ion beams facility at triumf," *Nuclear Instruments and Methods in Physics Research Section B: Beam Interactions with Materials and Atoms*, vol. 126, no. 1, pp. 231–235, 1997.

[3] Y. Blumenfeld, T. Nilsson, and P. V. Duppen, "Facilities and methods for radioactive ion beam production," *Physica Scripta*, vol. T152, p. 014 023, Jan. 2013.

[4] J. Dilling *et al.*, "Mass measurements on highly charged radioactive ions, a new approach to high precision with titan," *International Journal of Mass Spectrometry*, vol. 251, no. 2, pp. 198–203, 2006.

[5] A. Lapierre *et al.*, "The titan ebit charge breeder for mass measurements on highly charged short-lived isotopes—first online operation," *Nuclear Instruments and Methods in Physics Research Section A: Accelerators, Spectrometers, Detectors and Associated Equipment*, vol. 624, no. 1, pp. 54–64, 2010.

[6] K. G. Leach *et al.*, "Electroweak decay studies of highly charged radioactive ions with titan at triumf," *Atoms*, vol. 5, no. 1, 2017.

[7] K. Leach *et al.*, "The titan in-trap decay spectroscopy facility at triumf," *Nuclear Instruments and Methods in Physics Research Section A: Accelerators, Spectrometers, Detectors and Associated Equipment*, vol. 780, pp. 91–99, 2015.

[8] A. T. Gallant *et al.*, "TITAN-EBIT — charge breeding of radioactive isotopes for high precision mass measurements," *Journal of Instrumentation*, vol. 5, no. 08, pp. C08009–C08009, Aug. 2010.

[9] S. Ettenauer *et al.*, "In-trap decay spectroscopy of radioactive nuclei at titan/triumf for a determination of $2\nu\beta\beta$ matrix elements," *AIP Conference Proceedings*, vol. 1182, no. 1, pp. 100–103, 2009.

[10] Leach, K.G. *et al.*, "Sensitivity increases for the titan decay spectroscopy program," *EPJ Web of Conferences*, vol. 93, p. 07 006, 2015.

[11] H. R. Andrews *et al.*, *Proposal for a national facility: the 8π spectrometer. Proposition pour un détecteur national - le spectromètre 8π*. Chalk River, Ontario: Canada. At. Energy Comm., 1984.

[12] A. Pálffy, J. Evers, and C. H. Keitel, "Isomer triggering via nuclear excitation by electron capture," *Phys. Rev. Lett.*, vol. 99, p. 172 502, 17 Oct. 2007.

[13] A. Pálffy, W. Scheid, and Z. Harman, "Theory of nuclear excitation by electron capture for heavy ions," *Phys. Rev. A*, vol. 73, p. 012 715, 1 Jan. 2006.

[14] C. J. Chiara *et al.*, "Isomer depletion as experimental evidence of nuclear excitation by electron capture," *Nature*, vol. 554, no. 7691, pp. 216–218, Feb. 2018, ISSN: 1476-4687.

[15] Y. Wu, C. H. Keitel, and A. Pálffy, "^{93m}Mo Isomer depletion via beam-based nuclear excitation by electron capture," *Phys. Rev. Lett.*, vol. 122, p. 212 501, 21 May 2019.

[16] J. Ringuette, *Ph.d. thesis*, Colorado School of Mines, 2022, to be published.

[17] J. Kramp *et al.*, "Nuclear two-photon decay in 0+→0+ transitions," *Nuclear Physics A*, vol. 474, no. 2, pp. 412–450, 1987.

[18] J. Schirmer *et al.*, "Double gamma decay in ^{40}Ca and ^{90}Zr," *Phys. Rev. Lett.*, vol. 53, pp. 1897–1900, 20 Nov. 1984.

[19] E. R. Mucciolo and O. Helene, "Double gamma decay in ^{90}Zr," *Phys. Rev. C*, vol. 40, pp. 2403–2405, 5 Nov. 1989.

[20] J. Henderson *et al.*, "Upper limit on the two-photon emission branch for the $0_2^+ \rightarrow 0_1^+$ transition in ^{98}Mo," *Phys. Rev. C*, vol. 89, p. 064 307, 6 Jun. 2014.

[21] A. C. Hayes, J. L. Friar, and D. Strottman, "Two-photon decay of the first excited 0^+ state in ^{16}O," *Phys. Rev. C*, vol. 41, pp. 1727–1735, 4 Apr. 1990.

[22] J. Wood, E. Zganjar, C. De Coster, and K. Heyde, "Electric monopole transitions from low energy excitations in nuclei," *Nuclear Physics A*, vol. 651, no. 4, pp. 323–368, 1999.

[23] W. Witt *et al.*, "Sub-shell closure and shape coexistence in the

ISBN: 978-3-95450-239-4 ISSN: none doi: 10.18429/JACoW-EBIST2022-WE4WH03

transitional nucleus ^{98}Zr," *Phys. Rev. C*, vol. 98, p. 041 302, 4 Oct. 2018.

[24] E. Leistenschneider *et al.*, "Diversifying beam species through decay and recapture ion trapping: A demonstrative experiment at TITAN-EBIT," *Journal of Physics G: Nuclear and Particle Physics*, vol. 47, no. 4, p. 045 113, Mar. 2020.

ISBN: 978-3-95450-239-4 ISSN: none doi: 10.18429/JACoW-EBIST2022-WE4WH04

ABSOLUTE NUCLEAR CHARGE RADIUS MEASUREMENTS WITH EUV SPECTROSCOPY AT TITAN EBIT *

Y. Wang[†1], J. D. Cardona[2], A. A. Kwiatkowski[3], TRIUMF, Vancouver, Canada
R. Silwal, Appalachian State University, Boone, USA
E. Takacs, Clemson University, Clemson, USA
A. Lapierre[4], FRIB, East Lansing, USA
G. Gwinner, University of Manitoba, Winnipeg, Canada
[1]also at University of British Columbia, Vancouver, Canada
[2]also at University of Manitoba, Winnipeg, Canada
[3]also at University of Victoria, Victoria, Canada
[4]also at NSCL, East Lansing, USA

Abstract

Nuclear charge radii, a quantity crucial in many nuclear physics studies, can be extracted from Li-like electronic transitions, even in heavy ions, when combined with atomic theory [1,2]. This has progressed to permit such calculations from transitions in Na-like ions [3,4]. Charge breeding to Na-like charge state eases experimental requirements. To this end, at TRIUMF's Ion Trap for Atomic and Nuclear science (TITAN) facility, we are developing a high-efficiency, flat-field grazing incidence extreme-ultraviolet (EUV) spectrometer, for the measurement of absolute nuclear charge radii of short-lived nuclides. It will be installed to the Electron Beam Ion Trap (EBIT), which is capable of electron beam energies up to 66 keV. The spectrometer is designed to optimize transmission efficiency in the EUV regime. The ray-tracing simulations done in Shadow3 [5] will be presented. The first measurement candidates are ^{211}Fr and a suitable spin-0 isotope of Ra. These two elements are relevant for atomic parity violation (APV) experiments and searches for time-reversal violating permanent electric dipole moments (EDM).

INTRODUCTION

The nuclear charge radius is a fundamental property of the nucleus, and it plays a key role in understanding nuclear and atomic phenomena. Accurate measurement of nuclear charge radii is vital to understand nucleon-nucleon interactions, the appearance of non-traditional magic numbers, the onset of deformation, and the structure of exotic halo nuclei [6, 7]. Precision atomic tests of fundamental symmetries, such as atomic parity violation (APV) or searches for permanent electric dipole moments (EDM) as a signature of time reversal violation, require knowledge of nuclear charge distributions to extract the weak interaction physics from the measurement.

Some standard methods available to measure the absolute charge radius include elastic electron scattering [8] and muonic atom spectroscopy [9]. However, these techniques require macroscopic samples, exceeding by orders of magnitude the amount of short-lived radioactive isotopes that can be accumulated at radioactive beam facilities.

The critical ingredients to measure the absolute nuclear charge radius of short-lived heavy isotopes are access to intense radioactive ion beams (RIB), charge breeding to Na-like or higher charge states, optical access to the stored highly charged ions, and finally a spectrometer matched to the EUV light. All of these ingredients are united at TITAN [10], making it presently the only facility in the world capable of such measurements. Our first candidates are ^{211}Fr and a suitable spin-0 isotope of Ra. These two elements are of interest for APV experiments and the searches for EDM. We plan to probe the light emitted from the $3s\ ^2S_{1/2} - 3p\ ^2P_{1/2}$ ($D1$) transition of Na-like Fr and Ra isotopes to measure the energy emitted from this electronic transition. This specific transition is chosen as it offers the strongest optical signal, which is in the EUV regime, hence the necessity for a spectrometer that is highly sensitive to the EUV light. We will also probe the same transition from several isotopes of elements with well-known charge radii charge bred to the same charge state, which are used as references. We will then compare the energy shift with the expected theoretical energy difference, and obtain the charge radius of the isotope being measured by adjusting it in the theoretical calculation to match the measured transition energy shift.

In this proceeding, we describe the status and outlook of this nascent program.

EUV SPECTROSCOPY WITH TITAN EBIT

The TITAN EBIT [11] permits electron beams with currents up to 5 A and energies up to 66 keV. The Helmholtz style magnet allows optical access through seven radial ports. On one of these ports an EUV spectrometer will be installed. We have designed our spectroscopy setup, as illustrated in Figure 1. It will contain three major components: the EUV focusing optics, the EUV monochromator, and the charge coupled device (CCD) camera, where two key optical elements in the EUV monochromator will be an entrance slit and a grating substrate.

* Work supported by the Natural Sciences and Engineering Research Council (NSERC) of Canada and the National Research Council (NRC) of Canada through TRIUMF.

† ywang@triumf.ca

ISBN: 978-3-95450-239-4 ISSN: none doi: 10.18429/JACoW-EBIST2022-WE4WH04

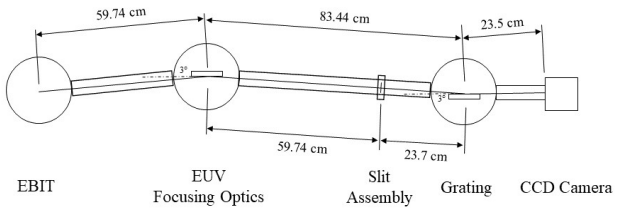

Figure 1: A sketch of the EUV spectroscopy setup that will be installed to the TITAN EBIT. Light collected from the EBIT will be focused and reflected by the focusing optics on the entrance slit, then diffracted by the grating substrate. The diffraction pattern will be collected by the CCD camera and analyzed.

The focusing optics will be a gold-plated, 15 cm long by 3.5 cm wide spherical mirror with a radius of curvature of 1141.471 cm. The center of the mirror will be placed 59.74 cm from the center of the EBIT chamber, at a grazing incidence angle of 3°. The mirror will collect light from the electronic transition in EBIT and concentrate it onto the bilateral entrance slit, with a continuously adjustable width from 0.001 to 3 mm [12]. There will be a 1:1 ratio between the source-to-mirror and the mirror-to-image distances. After passing through the entrance slit, the focused light will be diffracted by the spherical grating. The 50 mm by 30 mm flat-field grating with variable groove spacing will have a radius of curvature of 564.9 mm and nominal groove density of 1200 g/mm, which is ideal for the spectral range of 5 to 20 nm (62-248 eV) [13]. It will be located 23.7 cm from the entrance slit, at a grazing incidence angle of 3°. The diffraction pattern will be collected by the CCD camera, which will be placed in the focal plane of the grating, 23.5 cm away from the grating center [14].

We have commissioned the focusing optics and the monochromator from McPherson Inc. [12] for capabilities similar to the NIST EBIT's [14]. It will have a flat-field grazing incidence. The aspheric wavefront of the spherical substrate grating will allow corrections of aberration, thus providing high-resolution spectra. The device will be optimized for the range of 5-20 nm (62-248 eV) [15]. We have an existing CCD camera (iKon-L SO 936 series by Andor Technology), which offers a 2048 by 2048 array of active pixels, 13.5 by 13.5 μm in size, delivering a 27.6 by 27.6 mm active image area [16].

RAY-TRACING SIMULATIONS

The EUV spectrometer was simulated with SHADOW3, a widely used open-source ray-tracing program [5], through its recommended graphical environment, OrAnge SYnchrotron Suite (OASYS). Three optical elements (OE) were modelled: 1) geometrical source, 2) spherical mirror, and 3) spherical grating.

OE 1: Geometrical Source

We estimated a cylindrical ion cloud inside TITAN EBIT based on Herrmann theory [17, 18]. Since SHADOW3 only allows a one- or two-dimensional geometrical source, a cross section of the cylinder, a 0.01 cm by 7.0 cm rectangle, was used as the simulated source, with 25000 rays generated randomly through the Monte Carlo method. We chose a set of discrete photon energies, at 248 eV, 124 eV, 83 eV, and 62 eV (5 nm, 10 nm, 15 nm, and 20 nm). These energy values are chosen to correspond to the grating substrate in the monochromator, optimized for the 5 to 20 nm wavelength range as mentioned before, to examine the spatial separation of the diffraction pattern for photons with wavelengths in the EUV region of interest.

OE 2: Spherical Mirror

The gold plating of the spherical mirror was simulated through a pre-processor linked to an optical library that processes the reflectivity and transmission of the mirror [5], with the element of gold ($Z = 79$) and its density (19.32 g/cm^3) inputted as reflectivity parameters. This preliminary program generates the complex dielectric constant based on the user-defined mirror material from the atomic scattering factor library. The file is read and used by SHADOW to compute the local reflectivity based on Fresnel equations and phase shifts [19].

SHADOW allows users to define a continuation plane, where an image can be generated. This image then becomes the source for the next optical element, and is traced through to the final image position [19]. Such a continuation plane was created at the location of the entrance slit as shown in Figure 1. This serves as a virtual stopping point to examine the focused image at the slit, before passing the optical information to the spherical grating. The image generated at the continuation plane is shown in Figure 2. This focused image of the rectangular geometrical source serves as a validation that the optical parameters of the spherical mirror, including its position and its radius of curvature, are appropriately chosen.

OE 3: Spherical Grating

The spherical grating receives and processes information from the previous continuation plane. We simulate an imaging plane past the grating, at the location of the CCD camera in Figure 1, to visualize the diffraction pattern shown in Figure 3. We observe four spectral lines with distinct spatial separation, with larger spatial deviation corresponding to lower photon energy or longer wavelength.

This simulation modelled the optical path of the EUV light collected from the EBIT and processed by the spectrometer, and confirmed that the design of the optical elements in the spectroscopy setup is suitable.

STATUS AND OUTLOOK

The TITAN EBIT has been successfully operated for charge breeding of radioactive ion beams and in-trap spec-

ISBN: 978-3-95450-239-4 ISSN: none doi: 10.18429/JACoW-EBIST2022-WE4WH04

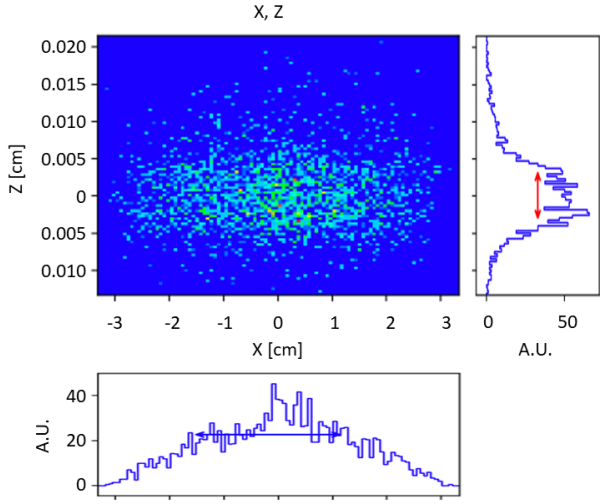

Figure 2: The focused image of the geometrical source at the entrance slit, simulated in SHADOW3.

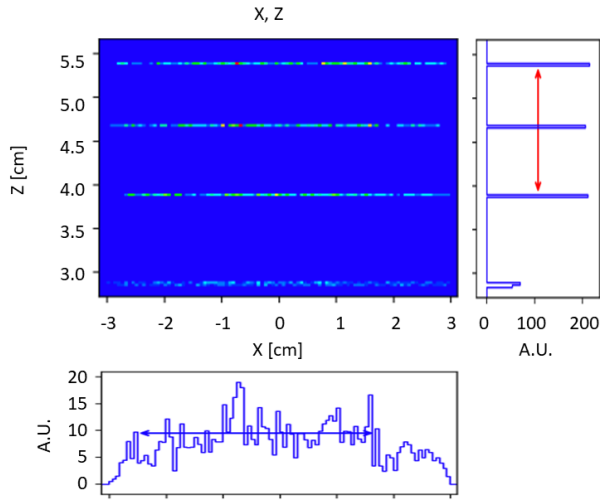

Figure 3: Spectral lines collected in SHADOW3 at the position of the CCD camera, spatially separated by the diffraction grating. From bottom to top, each line corresponds to photon energies of 248 eV (5 nm), 124 eV (10 nm), 83 eV (15 nm), and 62 eV (20 nm).

troscopy for more than a decade. These efforts have hitherto been focused either to support Penning trap mass spectrometry or focused on more traditional nuclear-physics studies. The addition of a newly commissioned EUV spectrometer from McPherson will expand TITAN's capabilities to include absolute and relative determination of nuclear charge radii. SHADOW3 simulations were performed to determine the optical properties required of the spectrometer system. Aside the spectrometer, the TITAN facility is otherwise experiment ready. With off-line tests of the spectrometer planned in fall 2022 and installation in spring 2023, the spectrometer should be ready for on-line experiments by summer 2023. The first measurements will validate the method using a suitable ion of a stable, heavy element with a well-determined nuclear charge radius. Subsequently, we plan to measure Ra and Fr relative to this anchor.

REFERENCES

[1] V. A. Yerokhin, P. Indelicato, and V. M. Shabaev, "Nonperturbative calculation of the two-loop Lamb shift in Li-like ions," *Physical Review Letters*, vol. 97, dec 2006.

[2] A. Senchuk, *On the determination of absolute nuclear charge radii for elements without stable isotopes via precision X-ray spectroscopy of lithium-like ions*. PhD thesis, University of Manitoba, 2018.

[3] J. D. Gillaspy, D. Osin, *et al.*, "Transition energies of the *D* lines in Na-like ions," *Phys. Rev. A*, vol. 87, p. 062503, Jun 2013.

[4] R. Silwal, A. Lapierre, *et al.*, "Measuring the difference in nuclear charge radius of Xe isotopes by EUV spectroscopy of highly charged Na-like ions," *Phys. Rev. A*, vol. 98, p. 052502, Nov 2018.

[5] M. S. del Rio, N. Canestrari, *et al.*, "*SHADOW3*: a new version of the synchrotron X-ray optics modelling package," *Journal of Synchrotron Radiation*, vol. 18, pp. 708–716, Sep 2011.

[6] K. Blaum, J. Dilling, and W. Nörtershäuser, "Precision atomic physics techniques for nuclear physics with radioactive beams," *Physica Scripta Volume T*, vol. T152, 01 2013.

[7] I. Angeli and K. P. Marinova, "Table of experimental nuclear ground state charge radii: An update," *Atomic Data and Nuclear Data Tables*, vol. 99, pp. 69–95, Jan. 2013.

[8] R. Hofstadter, "Electron scattering and nuclear structure," *Rev. Mod. Phys.*, vol. 28, pp. 214–254, Jul 1956.

[9] G. Fricke, C. Bernhardt, *et al.*, "Nuclear ground state charge radii from electromagnetic interactions," *Atomic Data and Nuclear Data Tables*, vol. 60, no. 2, pp. 177–285, 1995.

[10] A. Kwiatkowski, C. Andreoiu, *et al.*, "TITAN: An ion trap facility for on-line mass measurement experiments," *Hyperfine Interactions*, vol. 225, 10 2013.

[11] J. Cardona, "Updates on the TITAN EBIT," in *14th International Symposium on Electron Beam Ion Sources and Traps*, 2022 [Online].

[12] McPherson Inc., Chelmford, MA, USA, *Model 251MX PDF Data Sheet*.

[13] McPherson Inc., Chelmsford, MA, USA, *Model 251MX Grating Selection*.

[14] B. Blagojević, E.-O. Le Bigot, *et al.*, "A high efficiency ultra-high vacuum compatible flat field spectrometer for extreme ultraviolet wavelengths," *Review of Scientific Instruments*, vol. 76, no. 8, p. 083102, 2005.

[15] M. Wünsche, S. Fuchs, *et al.*, "A high resolution extreme ultraviolet spectrometer system optimized for harmonic spectroscopy and XUV beam analysis," *Review of Scientific Instruments*, vol. 90, no. 2, p. 023108, 2019.

[16] Andor Technology, Belfast, UK, *iKon-L SO*.

[17] F. Currell and G. Fussmann, "Physics of electron beam ion traps and sources," *IEEE Transactions on Plasma Science*, vol. 33, no. 6, pp. 1763–1777, 2005.

ISBN: 978-3-95450-239-4 ISSN: none doi: 10.18429/JACoW-EBIST2022-WE4WH04

[18] G. Herrmann, "Optical theory of thermal velocity effects in cylindrical electron beams," *Journal of Applied Physics*, vol. 29, no. 2, pp. 127–136, 1958.

[19] *SHADOW Primer (Upgraded to SHADOW3).*

ISBN: 978-3-95450-239-4 ISSN: none doi: 10.18429/JACoW-EBIST2022-TH1WH02

PERFORMANCE OF ANL EBIS AND RADIOACTIVE BEAM PRODUCTION*

R. Vondrasek†, C. Dickerson, J. McLain, B. Mustapha, G. Savard, R. Scott,
Argonne National Laboratory, Lemont, IL, United States

Abstract

Operation of the Argonne National Laboratory Electron Beam Ion Source (EBIS) was paused in March 2020 due to COVID restrictions. Source operation resumed in March 2022 with a focus on elongating the extracted beam pulse while maintaining high breeding efficiency. Through modification of the trap emptying waveform, a 10 ms pulse of $^{133}Cs^{27+}$ with a single charge state breeding efficiency of 22.2% has been achieved.

EBIS

Description

The EBIS charge breeder was designed in collaboration with Brookhaven National Laboratory and is based upon the RHIC TestEBIS [1]. Several parameters such as the electron gun, potential distribution in the ion trap region, electron collector, and injection/extraction systems were modified from those used for the TestEBIS with the goals of a shortened breeding time, higher transverse ion acceptance, and higher breeding efficiency [2, 3].

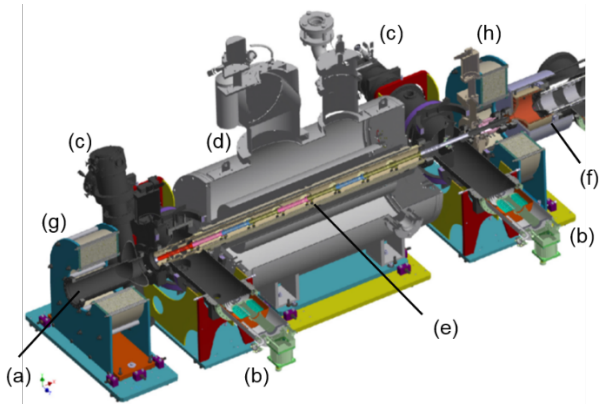

Figure 1: Overview of the EBIS charge breeder showing: a) electron gun, b) cryogenic pumps, c) turbomolecular pumps, d) 6 T superconducting solenoid, e) drift tube structure, f) electron collector, g) electron gun solenoid coil, h) collector solenoid coil.

The EBIS has turbomolecular and cryogenic pumps installed at either end of the trap and non-evaporable getter (NEG) strips installed along the length of the trap (Fig. 1). The trap operating pressure is < $1x10^{-10}$ Torr with the beamline operating at $1x10^{-9}$ Torr. A surface ionization source provides beams of $^{133}Cs^{+}$ for device tuning and charge breeding studies. A pulsed electric steerer after the surface source produces a beam pulse of 50 µs [4]. The electron beam is normally operated at 1.2 A, but for this series of measurements operation was reduced to 0.35 A, together with an increase in duty cycle to 60%. While trap capacity was reduced, measurements showed a relatively low electron beam neutralization factor of 2.5% during the breeding cycle. Source operating parameters are shown in Table 1.

Table 1: EBIS Parameters Used for Pulse Lengthening Series of Measurements

Magnetic field in trap	5.5 T
Magnetic field on cathode	0.15 T
IrCe cathode diameter	4.2 mm
Electron beam current	0.35 A
Electron beam diameter in trap	0.692 mm
Electron beam density in trap	92 A/cm2
Electron beam energy in trap	8951 eV
Drift tube diameter	20 mm
Trap length	0.532 m
Trap capacity	3.5 nC
Injection time	50 µs
Repetition rate	10 Hz
Duty cycle	60 %
EBIS high voltage bias	20 kV
Pressure (in trap)	<1x10-10 Torr

Beam Production

The EBIS started delivering radioactive beams for the ATLAS physics program in 2018. Beams produced to date have had an A/Q < 6, breeding times between 30-60 ms at 10 Hz repetition rate, and an average single charge state (SCS) breeding efficiency of 15.4% with a maximum of 24.6% (Table 2). The source has a substantially reduced beam contaminant level when compared to the ECR charge breeder it replaced [5]. The radioactive species (RIB Content) typically account for > 70% of the beam incident on target, whereas with the ECR the fraction was < 3%. Beam contaminants are volatile species such as fluorine or potassium with additional constituents arising from the 316L stainless steel components and the copper electron collector [6]. The charge state selected for beam delivery can typically be adjusted to avoid these known contaminants.

ISBN: 978-3-95450-239-4 ISSN: none doi: 10.18429/JACoW-EBIST2022-TH1WH02

Table 2: Beams Produced With ANL EBIS

Ion	SCS Efficiency (%)	Global Efficiency (%)	RIB Content (%)	Contaminant
$^{100}Zr^{21+}$	19.9	90	55	^{19}F
$^{102}Nb^{21+}$	13.8	93	91.3	^{41}K
$^{104}Nb^{21+}$	10.9	71		
$^{104}Mo^{20+}$		84		
$^{106}Mo^{20+}$	20.9	92	94.5	^{16}O
$^{110}Ru^{21+}$	21	96	98.6	^{68}Zn
$^{134}Te^{28+}$			99	None
$^{135}Te^{26+}$	9	66		
$^{138}I^{25+}$	7.5	40	96	^{116}Sn
$^{132}Xe^{27+}$				
$^{133}Cs^{27+}$	24.6	97		
$^{142}Cs^{26+}$	19.9	86	34.2	^{120}Sn, ^{121}Sb
$^{143}Ba^{28+}$	19.4	79	95.9	^{122}Sn, ^{123}Sb
$^{144}Ba^{28+}$	19	85	37.4	^{31}P
$^{144}La^{29+}$	5.9	85		
$^{146}La^{27+}$	10.3	67	100	None
$^{150}Ce^{29+}$	14	81	95.3	^{31}P

Work with the EBIS was paused in March 2020 due to COVID restrictions. During that time, a power failure damaged the chiller that cooled the helium compressor for the 6T solenoid. The parts necessary to affect a repair were not available until September 2021. EBIS operation resumed in March 2022 with this series of measurements focusing on elongating the extracted beam pulse.

Beam Pulse Extraction and Elongation

Charge bred beam can be extracted in one of two ways. The collector side barrier can be lowered within 1 μs to allow the highly charged ions to escape. This produces a 10-20 μs beam pulse. To reduce the high instantaneous rates and avoid detector pile up, techniques have been developed to slowly lower the barrier potential resulting in extracted pulse lengths of 80 ms [7, 8].

For the ANL EBIS, a trap-over-barrier extraction scheme has been implemented in which the potential of the trap electrodes is slowly ramped using an empirically tuned arbitrary function generator [9]. Once the energy of the individually trapped ions is high enough to overcome the collector side barrier potential, the ions spill out of the trap and are extracted. This scheme results in a reduced energy spread of the extracted ion beam since the total energy required to overcome the barrier potential is roughly constant. The beam pulse width is manipulated by varying the trap ramp waveform.

The original trap waveform utility specified low (filling) and high (emptying) trap voltages, width of the ramping pulse, and two log functions for shaping the waveform. This scheme produced 6 ms pulse widths, but the pulse uniformity was poor. Use of a single ramping waveform did not provide the flexibility to quickly ramp the trap voltage and still maintain a sufficiently flattened voltage during the critical emptying phase (Fig. 2).

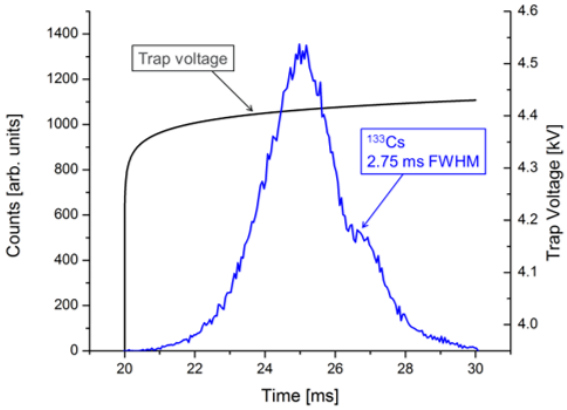

Figure 2: Pulse width with one-component trap emptying waveform.

An intermediate step utilized a BK Precision "Wave Express" software package [10] for waveform creation. However, the interface between the laptop-based program and the EBIS control system resulted in waveform update times of 5 minutes. The "Wave Express" utility did allow us to converge upon a satisfactory solution of two waveforms with independent variables.

A new waveform generator utility was developed by the EBIS control system group and allows for real-time changing of the trap ramping waveform. The waveform is divided into two components with independent control over their voltages, duration, and shaping. An ideal solution was arrived at where during the breeding cycle, the first waveform slowly ramps the trap to a voltage slightly below that necessary for emptying. The second waveform is then applied raising the trap the final ~50 V resulting in ion extraction. The optimum waveform raised the trap by 35 V in the first 0.5 ms and then gradually ramped the remaining 15 V over 9.5 ms giving insight into the trapped ion energy. A uniform beam pulse of 10 ms was achieved with a 22.2% SCS breeding efficiency (Fig. 3) while breeding efficiency with fast extraction mode (dropping the barrier) was 23.1%. Pulse widths of 20 ms with a uniform distribution of intensity have been achieved using this technique.

When the trap ramping cycle is complete, the electron beam is terminated, and the collector side barrier is lowered clearing the trap volume of any residual ions. In the case of Figure 3, these two beam pulses are visible. Their

ISBN: 978-3-95450-239-4 ISSN: none doi: 10.18429/JACoW-EBIST2022-TH1WH02

timing was shifted to ascertain how much beam was remaining in the trap near the end of the cycle and thus reduced the breeding efficiency.

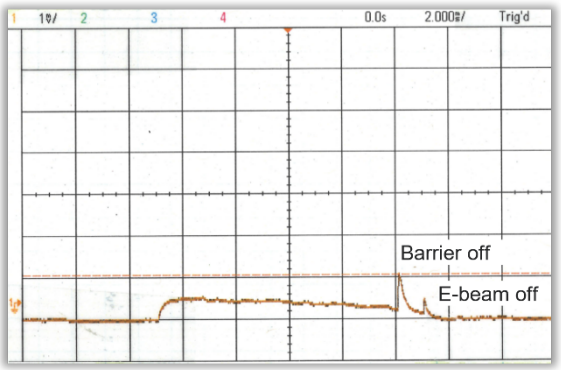

Figure 3: Pulse width with two-component trap emptying waveform.

NUCARIBU AND MULTI-USER

The CAlifornium Rare Isotope Breeder Upgrade (CARIBU) [11] provides radioactive beams to the Argonne Tandem Linac Accelerator System (ATLAS). Fission fragments are produced by a Cf-252 fission source located inside a large-volume RF/DC helium gas catcher [12]. The fragments are thermalized and rapidly extracted at up to 50 kV forming a low-energy beam of 1+ or 2+ ions.

The main obstacle with the passive Cf-252 source is that there is no longer a clear path forward to replace the depleted source, limiting the intensity capabilities of the low energy and reaccelerated CARIBU beams. Generating the neutron-rich isotopes with neutron induced fission on an actinide foil approach increases the isotope production intensities in some important regions, improves operation and maintenance simplicity, and provides a more reliable source [13]. Another unique feature of nuCARIBU is the capability of changing target foils to allow for production of fission fragments that are only available from fission of specific isotopes. Details and status of the program can be found elsewhere in these proceedings [14].

The ATLAS Multi-User Upgrade will take advantage of the continuous-wave nature of ATLAS and the pulsed nature of the EBIS charge breeder in order to simultaneously accelerate two beams with very close mass-to-charge ratios; one stable from the existing ECR ion source and one radioactive from the EBIS charge breeder [15]. An analysis of recent ATLAS operation data, when CARIBU beams are accelerated, shows that such an upgrade could deliver approximately 50% more beam time if certain experimental areas were equipped with appropriate instruments. The simultaneous acceleration of two beams produced by the EBIS with A/q separation of 1% ($^{133}Cs^{27+}$ via neutral gas injection and $^{132}Xe^{27+}$ via the surface ionization source) has been demonstrated with 70% transport efficiency.

CONCLUSION

Operation of the Argonne National Laboratory EBIS resumed in March 2022 with a focus on elongating the extracted beam pulse while maintaining high breeding efficiency. Through modification of the trap emptying waveform, a 10 ms pulse of 133Cs27+ with a single charge state breeding efficiency of 22.2% has been achieved. The waveform interface has improved flexibility and has allowed pulse widths as long as 20 ms with uniform distribution to be achieved. The nuCARIBU project and ATLAS Multi-User Upgrade projects are progressing with essential equipment arriving and installation plans being finalized.

This work was supported by the U.S. Department of Energy, Office of Nuclear Physics, under Contract No. DE-AC02-06CH11357. This research used resources of ANL's ATLAS facility, which is a DOE Office of Science User Facility.

REFERENCES

[1] A. Pikin, J. G. Alessi, E. N. Beebe, A. Kponou, R. Lambiase, R. Lockey, D. Raparia, J. Ritter, L. Snydstrup, and Y. Tan, 2010, JINST 5, C09003

[2] P. Ostroumov, S. Kondrashev, R. Pardo, G. Savard, R. Vondrasek, J. Alessi, E. Beebe, and A. Pikin, 2010, JINST 5, C07004

[3] P. N. Ostroumov, R. V. F. Janssens, M. P. Kelly, S. A. Kondrashev, B. Mustapha, R. C. Pardo, and G. Savard, in *Proceedings of XXV Linear Accelerator Conference*, Tsukuba, Japan, MOP045 (2010)

[4] P. N. Ostroumov, A. Barcikowski, C. A. Dickerson, A. Perry, A. I. Pikin, S. I. Sharamentov, R. C. Vondrasek, and G. P. Zinkann, Rev. Sci. Instrum. 86, 083311 (2015)

[5] R. Vondrasek, J. Clark, A. Levand, T. Palchan, R. Pardo, G. Savard, and R. Scott, Rev. Sci. Instrum. 85, 02B903 (2014)

[6] R. C. Vondrasek, C. A. Dickerson, M. Hendricks, P. Ostroumov, R. Pardo, G. Savard, R. Scott, and G. Zinkann, Rev. Sci. Instrum. 89, 052402 (2018)

[7] F. Wenander 2010 *JINST* 5 C10004

[8] A. Lapierre, Canadian Journal of Physics, 95(4), 361-369 (2017)

[9] Clayton Dickerson, Richard Vondrasek, Guy Savard, Daniel Santiago-Gonzalez, and Peter Ostroumov, AIP Conference Proceedings 2011, 070011 (2018)

[10] www.bkprecision.com/wavexpress.html

[11] R. Pardo, G. Savard, S. Baker, C. Davids, E. F. Moore, R. Vondrasek, G. Zinkann, Nucl. Instrum. Meth. B, 261, Issues 1-2, 965 (2007)

[12] G. Savard, Journal of Physics: Conference Series, 312, 052004 (2011)

[13] J. McLain, C. A. Dickerson, M. Gott, J. Greene, J. Nolen, G. Savard, J. Song, R. C. Vondrasek, 2022 J. Phys.: Conf. Ser. 2244 012062

[14] C. Dickerson, R. Gampa, J. Nolen, G. Savard, R. Vondrasek, TH1WH03, The nuCARIBU Upgrade to the ATLAS Reaccelerated Beam Program

[15] B. Mustapha, J.A. Nolen, G. Savard, P.N. Ostroumov, 2017 JINST 12 T12002

ISBN: 978-3-95450-239-4 ISSN: none doi: 10.18429/JACoW-EBIST2022-TH2WH02

STATUS OF THE CANREB EBIS AT TRIUMF

B. E. Schultz†, F. Ames, S. B. Beale, M. Cavenaile, C. R. J. Charles
TRIUMF, Vancouver, Canada V6T 2A3

Abstract

The CANadian Rare isotope facility with Electron Beam ion source (CANREB) is an essential part of the Advanced Rare IsotopE Laboratory (ARIEL) presently under construction at TRIUMF. CANREB can accept stable or rare isotope beams from a variety of ion sources, delivering high purity beams of highly charged ions (HCI) to experiments. The injected beams are bunched and cooled using a radiofrequency quadrupole (RFQ) cooler-buncher, and energy adjusted using a pulsed drift tube for injection into an electron beam ion source (EBIS) charge breeder. The EBIS was designed for a maximum electron beam current of 500 mA at a maximum magnetic field of 6 T. The EBIS can accept ion beam energies up to 14 keV and HCI with $3 < A/q < 7$ can be charge bred and extracted. The HCIs are separated using a Nier-type spectrometer before being transported to the linac for post acceleration. The status of the CANREB EBIS and recent results will be presented.

INTRODUCTION

TRIUMF houses a cyclotron which can produce proton beams at energies up to 520 MeV and currents up to 120 μA (> 300 μA total for all beamlines). For production of rare isotope beams (RIB), protons with energy 480 MeV (and currents up to 100 μA) impinge on targets comprised of U, Ta, Si, Th, Nb, or C [1]. Reaction products are formed through fission and spalation reactions and ionized using surface, laser, or plasma discharge ion sources. Ions are extracted at energies up to 60 keV and can be transported directly to low energy experiments in the Isotope Separator and ACcelerator (ISAC) facility. Ions can also be transported to high energy experiments (up to 15 MeV/nucleon for low A/q) following post-acceleration through a multi-stage (room temperature and superconducting) linac. The linac has an energy acceptance of 2.04 keV/nucleon, limiting the mass-to-charge ratio to $A/q = 30$ for 60 keV. Post-acceleration of heavier ions requires charge breeding to $3 < A/q < 7$. Currently, highly charged ions (HCI) are created using an electron cyclotron resonance ion source (ECRIS) installed in ISAC [2]. The ECRIS is limited to efficiencies of a few percent, and also generates high background currents due to high residual gas pressure and plasma chamber sputtering. The resulting isobaric currents can be several orders of magnitude more intense than the species of interest. The maximum achievable charge state from the ECRIS is also limited, and secondary stripping in the linac is often required to reach the necessary energy which further limits the efficiency.

The Advanced Rare IsotopE Laboratory (ARIEL) project is currently under construction at TRIUMF. In addition to adding two new target stations for RIB production, ARIEL also includes the CANadian Rare isotope facility with Electron Beam ion source (CANREB) for charge breeding of ions. CANREB utilizes an electron beam ion source (EBIS) to generate HCI. The EBIS is designed for ultrahigh vacuum operation, which greatly reduces the background contamination relative to the ECRIS. The EBIS can also reach higher charges states, mitigating the need for a second stripping and permitting the delivery of clean and intense post-accelerated beams to ISAC.

CANREB OVERVIEW

CANREB is located in the ARIEL building adjacent to ISAC (Fig. 1). The lower level of the ARIEL building contains the future mass separator room, which houses the CANREB high resolution separator (HRS). The HRS has a dual magnetic dipole which is designed to reach resolving powers up to 20000 [3]. The HRS can accept beam from the future ARIEL target stations, which is then transported upstairs through a vertical beamlime. If additional mass separation is not required, the HRS can be bypassed. The HRS is currently being commissioned off-line. The mass separator room also contains the ARIEL test ion source (TIS) [4], a small surface source used for stable beam tests in CANREB.

The CANREB charge breeding systems are located on the ground floor of the ARIEL building. Stable ion beams can be injected from the TIS or from the off-line ion source (OLIS) in ISAC. RIB can currently be injected from the ISAC target stations and from ARIEL in the future. Ions can be injected at energies up to 60 keV into the radiofrequency quadrupole (RFQ) cooler-buncher [5] with intensities up to a few 100 pA. The ions are confined using a combination of DC electric and RF fields ($f_{RF} = 3 - 6$ MHz) for up to 10 ms (at a nominal rep rate of 100 Hz). A helium buffer gas ($P \approx 30$ mTorr) cools the trapped ions. The extracted ions have a nominal FWHM width of ≈ 1 μs. The extracted ions must be reduced in energy for coupling into the charge breeder, which is accomplished using a pulsed drift tube (PDT). The PDT is rapidly switched between high voltage and ground using a push-pull Behlke switch (fall time < 500 ns).

The EBIS was designed and constructed at the Max Planck Institute for Nuclear Physics in Heidelberg, Germany [6]. The system is designed to accept ions with energies up to 14 keV (set by the desired A/q and the energy acceptance of the linac) and intensities up to $\sim 10^7$ particles per bunch at 100 Hz. The ions are confined electrostatically in the center of a split-bore, semi-Helmholtz superconducting (4 K) magnet with a maximum field strength of 6 T. A barium dispenser cathode generates an electron beam with an energy

†bschultz@triumf.ca

ISBN: 978-3-95450-239-4 ISSN: none doi: 10.18429/JACoW-EBIST2022-TH2WH02

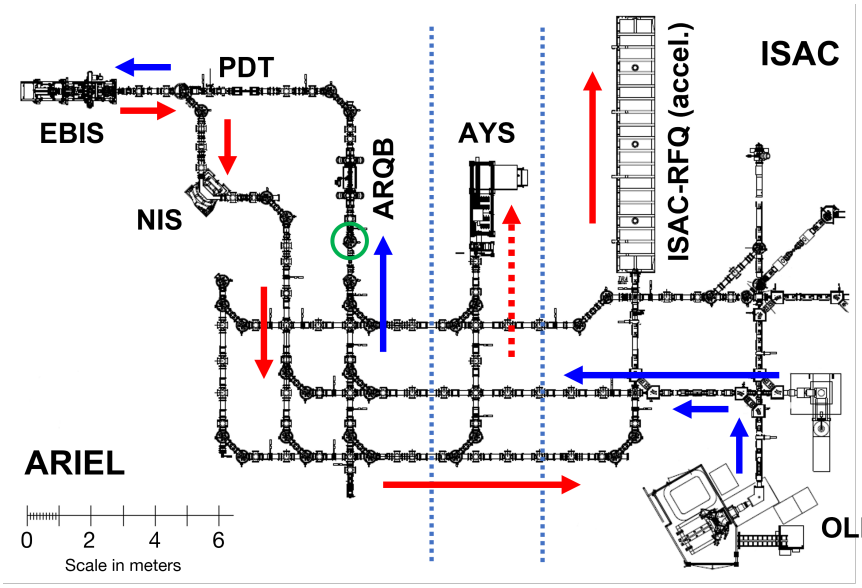

Figure 1: Layout of CANREB charge breeding systems. See text for acronym definitions. Blue arrows indicate path of beam injected into CANREB, either from OLIS or the ISAC target stations. Charge bred RIB from the EBIS can either be sent to the AYS for yield measurement (dashed red arrow) or into the ISAC linac for post-acceleration (solid red arrows). In the future, beam from the new ARIEL target stations can be injected into CANREB (green circle) and charge bred in the EBIS.

and current of up to 15 keV and 500 mA, respectively. The electron beam is compressed through the trapping region by the magnetic field before being deposited onto an electron collector. The drift tubes in the trapping region are cooled with the magnet to $\approx$ 4 K to act as a getter to reduce the residual gas pressure in the charge breeding region. Trapped ions are charge bred for up to 10 ms and are then extracted and transported through a Nier-type spectrometer (NIS) for charge state separation ($m/dm \approx 300$).

EBIS COMMISSIONING AND STATUS

For EBIS commissioning the ion beam energy—which is set by the high voltage (HV) bias of the central drift tubes—was limited to a maximum of 7 keV. In the presence of a strong magnetic field, higher voltages would lead to a persistent HV discharge, creating negative vacuum effects and voltage instabilities that rendered the system inoperable. The discharge was only present with the magnetic field turned on, which required the maximum field strength to be limited to 1 T. Attempts to address this issue following high voltage failures in 2019 and 2021 were only partially successful; investigations (and simulations [7]) are underway to try and solve the problem. In addition to voltage limitations, the electron gun current was limited to 40 mA.

The EBIS was commissioned using a number of ion beams. The TIS provided ^{85}Rb and ^{133}Cs beams at energies up to 30 keV. A variety of alkali (Rb, Cs) and noble gas beams (Kr, Ar) were injected from OLIS. Radioactive beams from an ISAC target station were also charge bred and successfully post-accelerated to a high energy experiment for tests [8].

An A/q spectrum of charge bred ^{85}Rb from OLIS is plotted in Fig. 2 (top), measured prior to the latest HV failure. The black and red spectra were measured with the Rb injected into the EBIS and blocked, respectively. The EBIS was operating with $B = 1$ T and an electron beam energy/current of 4.3 keV/27 mA. The ion energy was 6.3 keVxq and the charge breeding time was 8 ms. The spectra were recorded by varying the magnetic field of the NIS and recording the ion beam current on a downstream Faraday cup. The A/q-axis has been truncated to show the region of interest for post-acceleration. Figure 2 (bottom) shows the resulting charge state distribution (CSD) and relative abundances of the various charge states. In the peak of the CSD (roughly Rb 11+) the charge breeding efficiency was $\approx$ 2% with an injected beam current of 200 pA. For comparison, the CSD for an 8 ms charge breeding time was estimated using CBSIM [9]. The electron beam current density was adjusted to match the peak of the distribution, giving a value of 50 A/cm^2. For these electron beam parameters, the Herrmann radius was estimated to be 112 μm, giving a current density of $\approx$ 70 A/cm^2 which is consistent with CBSIM. The measured CSD is much broader than that generated by CBSIM, with lower and higher charge states. This could be caused by poor overlap of the ion cloud with the electron beam and/or the trap not being fully emptied after each charge breeding cycle.

The EBIS was recently brought back to an operational state following the latest HV failure. Figure 3 shows A/q

ISBN: 978-3-95450-239-4 ISSN: none doi: 10.18429/JACoW-EBIST2022-TH2WH02

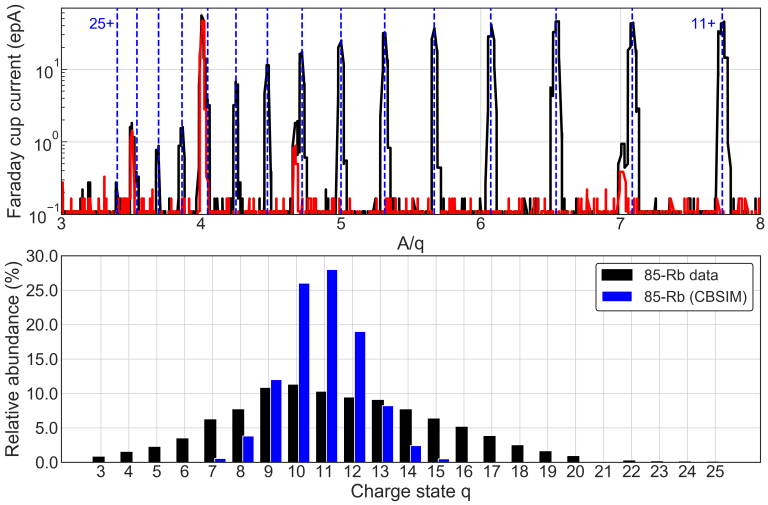

Figure 2: ^{85}Rb charge bred in the EBIS. Electron beam energy = 4.3 keV, electron beam current = 27 mA, magnetic field = 1 T, charge breeding time = 8 ms, and ion energy = 6.3 keVxq. (Top) A/q spectra with the Rb beam injected (black) and blocked (red). Blue dashed lines indicate position of Rb charge states from 11–25+. (Bottom) Charge state distribution and relative charge state abundances for measured data (black) and simulated data (blue).

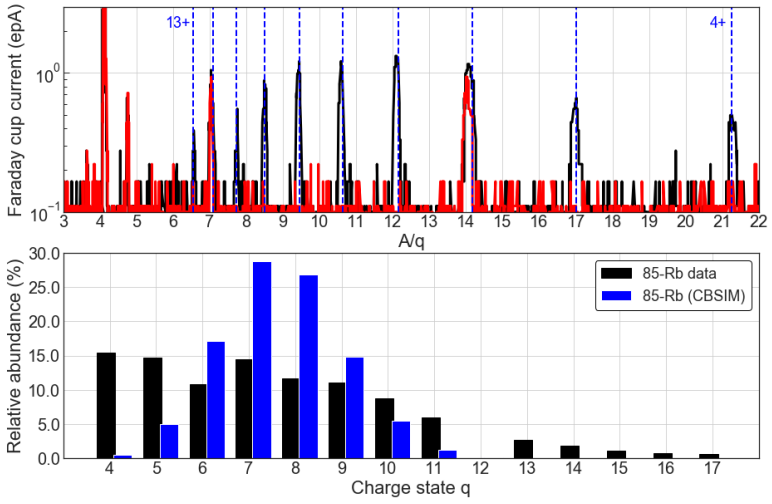

Figure 3: ^{85}Rb charge bred in the EBIS. Electron beam energy = 4.3 keV, electron beam current = 17 mA, magnetic field = 1 T, charge breeding time = 4 ms, and ion energy = 5.3 keVxq. (Top) A/q spectra with the Rb beam injected (black) and blocked (red). Blue dashed lines indicate position of Rb charge states from 4–13+. (Bottom) Charge state distribution and relative charge state abundances for measured data (black) and simulated data (blue).

spectra (top) and charge state distribution (bottom). The EBIS was operating with B = 1 T and an electron beam energy/current of 4.3 keV/17 mA. The ion energy was 5.3 keVxq and the charge breeding time was 4 ms. In the peak of the distribution (roughly Rb 7+) the charge breeding efficiency was < 0.1%. Similar to the data from 2021, the CSD is broad compared to that predicted by CBSIM, which could again indicate issues with ion trapping. The electron beam current density in CBSIM was 32 A/cm^2, compared to 44 A/cm^2 as estimated from theory.

CONCLUSION

CANREB has been built to charge breed stable and rare isotope beams using an EBIS for post-acceleration to high energy experiments in ISAC. CANREB systems have been commissioned, and the RFQ cooler-buncher, PDT, and NIS are all operating to specifications. A number of ion species have been charge bred in the EBIS for times up to 8 ms, achieving single charge state efficiencies up to ≈ 2% in the peak of the charge state distributions.

EBIS performance during commissioning was limited due to high voltage stability issues relating to discharge through

ISBN: 978-3-95450-239-4 ISSN: none doi: 10.18429/JACoW-EBIST2022-TH2WH02

the drift tube bias. The discharge was strongly correlated to the presence of the magnetic field. As a result, the ion beam energy was limited to < 7 keV x q at a maximum magnetic field of 1 T. These parameters were sufficient for commissioning, but will not allow the system to be operated within the full range required for beam delivery at TRIUMF (6–14 keV). Attempts to resolve this issue have up-to-now been largely unsuccessful, and efforts are underway to try and fix the problem. Once the high voltage can be operated to specification, efforts will focus on improving EBIS efficiency and overall performance.

REFERENCES

[1] *ISAC and ARIEL: The TRIUMF Radioactive Beam Facilities and the Scientific Program*, J. Dilling, R. Krücken and L. Merminga Ed. Dordrecht, Netherlands: Springer, 2014.

[2] F. Ames, R. Baartman, P. Bricault and K. Jayamanna, *Hyperfine Interact.*, vol. 225, pp. 63–67, 2014.

[3] M. Marchetto *et al.*, *Nucl. Instrum. Methods Phys. Res. B*, vol. 463, pp. 227–231, 2020.

[4] S. Saminathan, F. Ames, R. Baartman, M. Marchetto, O. Lailey and A. Mahon, *Rev. Sci. Instrum.*, vol. 90, pp. 123302, 2019.

[5] B. R. Barquest, J. C. Bale, J. Dilling, G. Gwinner, R. Kanungo, R. Krücken and M. R. Pearson, *Nucl. Instrum. Methods Phys. Res. B*, vol. 376, pp. 207–210, 2016.

[6] M. A. Blessenohl *et al.*, *Rev. Sci. Instrum.*, vol. 89, pp. 052401, 2018.

[7] C. R. J. Charles *et al.*, "Simulations of the CANREB EBIS: Where Might the Issue(s) Be?", presented at the 14th Int. Symp. of EBIS/T, Whistler, Canada, June 2022, this conference.

[8] B. E. Schultz, C. R. J. Charles, M. Cavenaile, R. Kanungo, F. Ames and O. Kester, *J. Phys.: Conf. Ser.*, vol. 2244, pp. 012028, 2022.

[9] R. Becker, O. Kester and Th. Stoehlker, *J. Phys.: Conf. Ser.*, vol. 58, pp. 443-446, 2007.

ISBN: 978-3-95450-239-4 ISSN: none doi: 10.18429/JACoW-EBIST2022-FR1WH03

COLLINEAR LASER SPECTROSCOPY OF $^{12}C^{4+}$: TOWARDS AN ALL-OPTICAL NUCLEAR CHARGE RADIUS DETERMINATION

P. Imgram*, K. König, P. Müller, W. Nörtershäuser
Institute for Nuclear Physics, Technical University of Darmstadt, [64289] Darmstadt, Germany
B. Maaß
Physics Division, Argonne National Laboratory, [60439] Lemont, IL, USA

Abstract

Recent progress in non-relativistic QED calculations for He-like atomic systems opens up the possibility of all-optical nuclear charge radius determinations beyond He. Therefore, $1s2s\,^3S_1 \rightarrow 1s2p\,^3P_J$ transitions in $^{12}C^{4+}$ are investigated as a proof-of-principle experiment. Here, first collinear laser spectroscopy resonance spectra of $^{12}C^{4+}$ from an electron beam ion source (EBIS) are presented and peak shapes are studied for different EBIS production modes.

INTRODUCTION

The investigation of the nuclear size plays an important role in the unraveling of the nuclear structure since its discovery by Rutherford. Different techniques have been developed over time to measure the nuclear mean square charge radius $\langle r^2 \rangle$ [1]. For stable nuclei, the nuclear charge distribution can directly be probed through elastic electron scattering [2]. Also myonic atom spectroscopy has been proven a valuable tool for the extraction of nuclear size information [3]. For radioactive nuclei, one had to come up with a procedure which takes only few ms from the production of the unstable nuclei to the measurement. Therefore, Collinear Laser Spectroscopy (CLS) has been developed [4] and since then established as a workhorse in this field [5, 6]. It unites high resolution with a fast measurement cycle through in-flight spectroscopy on fast ions (10 - 60 keV) in a collinear geometry. However, laser spectroscopy of radioactive nuclei only yields changes $\delta\langle r_c^2 \rangle$ of the nuclear ms charge radii along an isotopic chain. In order to obtain the nuclear size $\langle r^2 \rangle$ also for short-lived isotopes, a combined analysis of all available measurements is used [1]. Due to major advances in non-relativistic QED (NRQED) calculations in one- and two-electron-systems in the past years they are now chiefly limited by the finite nuclear-size effect. This means that the nuclear size can be determined in an all-optical way through a comparison between a measured transition frequency ν_0 and the calculated frequency ν_{point} in the respective transition under assumption of a point-like nucleus. This has been demonstrated in H [7, 8], μH [9] and μHe so far [10] and also led to the famous proton radius puzzle [11]. The recent agreement between theory and experiment in the $2\,^3S_1 \rightarrow 2\,^3P_J$ in He reported in [12] opens up the possibility to expand this approach of all-optical nuclear charge radii also to He-like ions of heavier species. Unfortunately, the lifetime of the metastable $2\,^3S_1$ state decreases quickly with increasing nuclear charge Z as shown in Table. 1. Similar to short-lived nuclei, CLS is the best-suited method to investigate the corresponding transitions in He-like Be, B and C ions. Beginning with N the wavelength is not accessible with commercial laser systems anymore but might be available at some point. Furthermore, the determination of the stable nuclei ^{10,11}B with this all-optical approach is of special interest since it promises much better accuracy compared to elastic electron scattering which is hindered by the interference of the two form factor components C0 and C2 in these nuclei [13]. A precise charge radius measurement in these stable nuclei is crucial to deduce the possible proton-halo from ^{8}B [14, 15].

From all available candidates besides He, the nuclear charge radius of ^{12}C is known to highest precision from myonic atom spectroscopy [16] and elastic electron scattering [17] making $^{12}C^{4+}$ a perfect proof-of-principle candidate. Furthermore, ^{12}C is the only nucleus in this region without nuclear spin which simplifies the NRQED calculations as well as the experiment. In the following, the experimental setup will be explained and first resonance spectra of the $2\,^3S_1 \rightarrow 2\,^3P_2$ transition in $^{12}C^{4+}$ for different measurement parameters are shown and compared.

Table 1: Lifetime τ and Transition Wavelength λ of the Metastable $2\,^3S_1$ State in He-like Ions

Ion species	$\tau(2\,^3S_1)$	$\lambda(2\,^3S \rightarrow 2\,^3P)$
He	2.2 h	1082 nm
Li^+	50 s	548 nm
Be^{2+}	1.8 s	372 nm
B^{3+}	150 ms	282 nm
C^{4+}	21 ms	227 nm
N^{5+}	3.9 ms	190 nm

EXPERIMENTAL SETUP

The experiment is performed at the COllinear Apparatus for Laser spectroscopy and Applied science (COALA) situated at the Institute for Nuclear Physics of the Technical University of Darmstadt. The technique of (quasi-)simultaneous collinear and anti-collinear laser spectroscopy [18] has been established and improved at COALA in previous experiments [19–21]. Although a few improvements and changes of the setup have been carried out over the past years, the measurement principle and main parts of the beamline are are still as detailed in [22]. Therefore, only a brief sum-

* pimgram@ikp.tu-darmstadt.de

ISBN: 978-3-95450-239-4 ISSN: none doi: 10.18429/JACoW-EBIST2022-FR1WH03

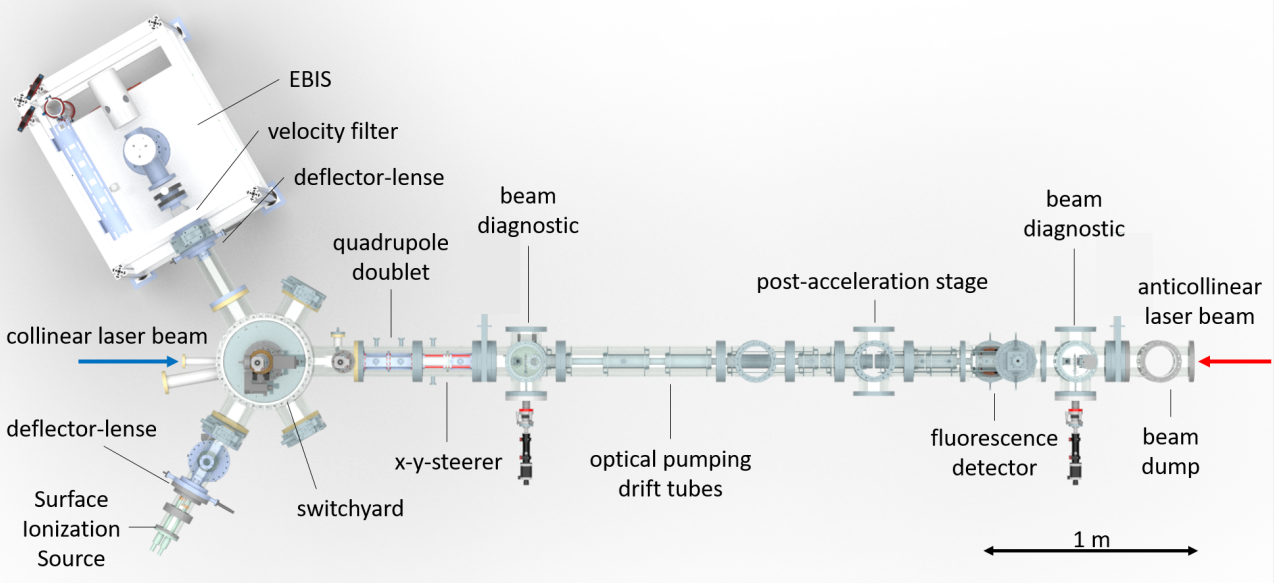

Figure 1: Schematic model of the COALA beamline. Details to the beamline can be found in [22]. A new development is the switchyard which allows more flexibility for parallel usage of ion sources. An electron beam ion source EBIS-A from Dreebit has been installed to investigate light He-like ions.

mary is given here.

The current setup of the COALA beamline is depicted in Fig. 1 and shows two major changes in comparison to [22]. First, a new switchyard has been installed to provide more flexibility regarding the parallel usage of ion sources. Second, a new electron beam ion source EBIS-A from DREEBIT including a velocity filter has been installed and commissioned at COALA. It is fed with methane gas to charge breed carbon ions. During this process the metastable $2\,^3S_1$ state of the $^{12}C^{4+}$ ions is proportionally populated mainly by charge exchange with neutral atoms and C^+. The produced particles with charge q and mass A leave the EBIS with a kinetic energy of about 10.5 keV/q and are selected by A/q through the following velocity filter. This results in $^{12}C^{4+}$ ion bunches of roughly $10^7 - 10^8$ ions/bunch with a repetition rate of ≈ 60 Hz which corresponds to typical breeding times of about 15 ms. Alternatively, the voltage of the ejection electrode can be permanently lowered allowing ions to continuously leak from the EBIS. In this way, a continuous ion beam of about 1.4 nA is obtained. Afterwards, the ions are injected in to the main beamline by applying a high voltage to deflection electrodes in the switchyard. A following quadrupole doublet and an x-y-steerer enable ion beam shaping and positioning. Iris diaphragms in two beam diagnostic stations before and after the optical detection region (ODR) ensure a well defined superposition of the ion and the laser beams. When the laser frequency $\nu_{c/a}$ in the ions rest-frame matches the transition frequency ν_0, the ions are excited to the $2\,^3P_J$ states with a lifetime of 17 ns and emit fluorescence light during the decay. These photons are collected with a mirror system covering nearly 4π [23], counted with fast photomultiplier tubes, and are processed with a time resolution of 10 ns with a FPGA based data acquisition. Due to the velocity $\beta = v/c$ of the ions, the resonance condition is shifted for a counter-propagating (anticollinear, a) and co-propagating (collinear,c) laser beam by the relativistic Doppler effect according to

$$\nu_{c/a} = \nu_0 \gamma (1 \pm \beta)$$

with the Lorentz factor $\gamma = 1/\sqrt{1-\beta^2}$. This condition can either be met by scanning the laser frequency or by changing the ion velocity by applying a few 10 V to the ODR, which can be floated relative to the rest of the beamline. Usually the latter is easier and faster and therefore the preferred method. The precise determination of the rest-frame transition frequency ν_0 would require a precise knowledge of the ion velocity β if only ν_a or ν_c is measured. However, if the laboratory-frame transition frequencies ν_c and ν_a are measured in fast iteration, this allows us to directly access ν_0^2 through.

$$\nu_c \nu_a = \nu_0^2 \gamma^2 (1+\beta)(1-\beta) = \nu_0^2$$

RESONANCE SPECTRA

A first step towards the determination of the rest-frame transition frequency in the $2\,^3S_1 \rightarrow 2\,^3P_2$ transition of $^{12}C^{4+}$ ions is the optimization of EBIS parameters with respect to the appearance of the optical resonance spectra. Therefore, a 1-mW laser beam at a wavelength of 227 nm was superposed in anticollinear geometry with the ions and brought into resonance by scanning the voltage applied to the ODR. The more commonly used bunch-mode operation of the EBIS was studied first and then compared to continuous-beam (leaky-mode) operation of the EBIS.

ISBN: 978-3-95450-239-4 ISSN: none doi: 10.18429/JACoW-EBIST2022-FR1WH03

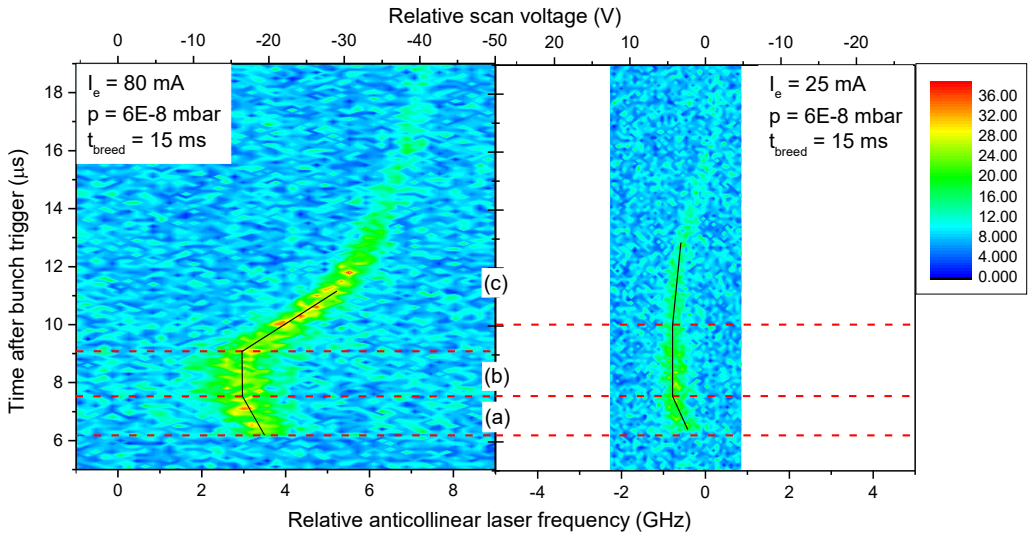

Figure 2: Time-resolved spectra for two different EBIS electron currents. The fluorescence intensity detected with the photomultipliers (color coded) is depicted as a function of the laser frequency (x-axis) and the arrival time of the ions with respect to the extraction pulse (y-axis). Three different parts (a,b,c) can be identified in each bunch (see text). Less electron current results in a reduced negative space charge and a colder ion cloud, which improves the shape and the width of the optical spectrum. Therefore the right spectrum is preferred against the left one for precision CLS measurements despite the smaller number of ions.

Bunched Beam

In the bunched mode the ion cloud is stored for a certain breeding time t_{breed} in the EBIS and afterwards ejected by fast ramping the extraction-electrode potential below the trap potential. Further important parameters which influence the ion production are the ion current I_{e}, the trap potential ΔU_{Trap} and the methan pressure p inside the EBIS. The left panel in Fig. 2 shows a time-resolved resonance spectrum contour plot for $I_{\mathrm{e}} = 80\,\mathrm{mA}$, $\Delta U_{\mathrm{trap}} = 70\,\mathrm{V}$, $p = 6 \cdot 10^{-8}$ mbar and $t_{\mathrm{breed}} = 15\,\mathrm{ms}$. With these settings we achieved the largest number of $^{12}C^{4+}$ ions per bunch. Ideally, the resonance center would exhibit as a narrow feature and a straight vertical line in the time resolved spectrum. However, with these settings it shows a distinct time behaviour that is inappropriate for high precision CLS measurements. The drift of the resonance center with time is attributed to a change in kinetic energy of the ions. Analysing the observed spectrum in more detail, it can be roughly separated in three regions indicated by the red dashed lines: The ions in window (a) can already leave the trap while the potential of the extraction electrode is still changing. Hereby, the electrode acts as an elevator drift-tube where the ions lose energy and the resonance is therefore shifted to the right. The time window indicated (b) shows the required time-independent resonance frequency and can be used to extract a resonance spectrum through projection onto the frequency axis. The strongly tilted tail in region (c), now drifting towards lower ion energies can be explained with the space-charge potential of the electron beam. Those ions see an increasing part of the negative space charge potential of the electrons and therefore start on a lower acceleration potential than the ions that arrived earlier (in regions a and b). This influence becomes even more clear when compared to a setting with much lower electron current I_{e} shown in the right panel in Fig. 2. It is obvious that less ions are produced in total but the kinetic energy distribution is considerably smaller. Although still roughly three parts can be identified, the straight main bunch is now longer and narrower which is beneficial for a precise resonance frequency determination. Also the tilt of the tail (c) is less prominent due to the reduced negative space-charge potential. In total a lot of different combinations of production parameters have been tested in order to achieve an ion cloud that is as cold as possible in the EBIS. This requires that I_{e} and ΔU_{trap} should be as low as possible but still offering a sufficiently large ion production, while p should simply be as high as possible. The breeding time was typically set to $t_{\mathrm{breed}} = 15\,\mathrm{ms}$ since this yielded the most ions in the metastable $2\,^3S_1$ state and smallest linewidth.

Continuous Beam

After the successful demonstration of CLS in bunched-beam mode, the production of continuous beam of $^{12}C^{4+}$ in the metastable $2\,^3S_1$ state from the EBIS was investigated. Initially, it was not sure whether the metastable state will be sufficiently well populated under the breeding conditions in leaky mode operation but a CLS resonance was also observed as shown in Fig. 3. In comparison to the resonance spectra of the bunched mode the continuous beam spectrum has a reduced linewidth of roughly a factor five which also reduces the uncertainty of the transition frequency determination by the same factor. Note that both modes have a comparable signal-to-noise ratio although the resonances

ISBN: 978-3-95450-239-4 ISSN: none doi: 10.18429/JACoW-EBIST2022-FR1WH03

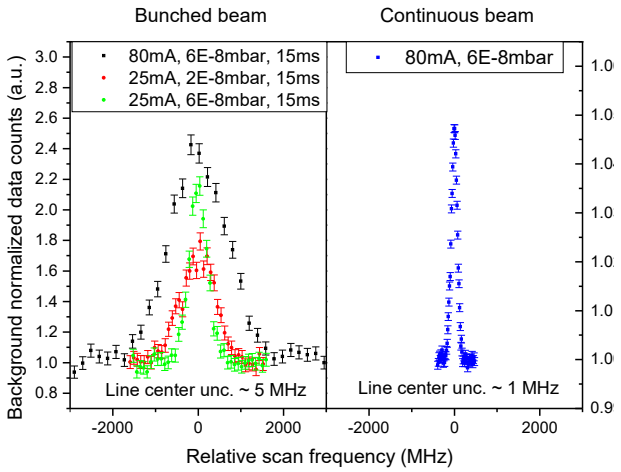

Figure 3: Comparison of resonance spectra taken in bunched-beam mode (left) and continuous-beam mode (right). The continuous spectrum has a linewidth and line-center uncertainty reduced by a factor of five. Even though the signal-to-background ratio is worse in the continuous mode, the signal-to-noise ratio is comparable for similar measurement times since the signal is concentrated into a smaller spectral range.

taken with bunched beams have a much better signal-to-background ratio. The reason for this is twofold: the relatively slow repetition rate of 60 Hz in bunched mode results in much less gathered photons/data point per real time compared to the continuous mode and the signal is compressed within a much narrower spectral range.

CONCLUSION

An electron beam ion source has been successfully installed and commissioned at the COALA setup in order to investigate the $2\,^3S_1 \rightarrow 2\,^3P_J$ transitions in $^{12}C^{4+}$. First optical resonance spectra were taken and compared for different production parameters and operation modes. Best results were achieved with a continuous ion beam resulting in statistical line center uncertainties of about 1 MHz. Thus, working conditions for a dedicated determination of the rest-frame transition frequencies through (quasi-)simultaneous collinear and anticollinear laser spectroscopy are established.

ACKNOWLEDGEMENTS

This project is supported by the German Research Foundation (Project-ID 279384907 – SFB1245) and the German Federal Ministry of Education and Research (Project-ID 05P21RDFN1).

REFERENCES

[1] G. Fricke, K. Heilig, and H. F. Schopper, "Nuclear charge radii," 2004, ISBN: 978-3-540-42829-9. DOI: 10.1007/b87879.

[2] R. Hofstadter, "Electron scattering and nuclear structure," *Reviews of Modern Physics*, vol. 28, no. 3, pp. 214–254, 1956, ISSN: 0034-6861. DOI: 10.1103/RevModPhys.28.214.

[3] E. Borie and G. A. Rinker, "The energy levels of muonic atoms," *Reviews of Modern Physics*, vol. 54, pp. 67–118, 1982, ISSN: 0034-6861.

[4] K. Anton *et al.*, "Collinear laser spectroscopy on fast atomic beams," *Phys. Rev. Lett.*, vol. 40, pp. 642–645, 1978.

[5] E. W. Otten, *Nuclear Radii and Moments of unstable Isotopes*, ser. Treatise on heavy ion science vol. 8: Nuclei far from stability. New York: Plenum Publishing Corp. (Springer), 1989, ISBN: 978-0306429491.

[6] P. Campbell, I. D. Moore, and M. R. Pearson, "Laser spectroscopy for nuclear structure physics," *Progress in Particle and Nuclear Physics*, vol. 86, pp. 127–180, 2016, ISSN: 0146-6410. DOI: 10.1016/j.ppnp.2015.09.003.

[7] A. Beyer *et al.*, "The rydberg constant and proton size from atomic hydrogen," *Science*, vol. 358, no. 6359, pp. 79–85, 2017. DOI: 10.1126/science.aah6677.

[8] A. Grinin *et al.*, "Two-photon frequency comb spectroscopy of atomic hydrogen," *Science*, vol. 370, no. 6520, pp. 1061–1066, 2020. DOI: 10.1126/science.abc7776.

[9] R. Pohl *et al.*, "The size of the proton," *Nature*, vol. 466, no. 7303, pp. 213–216, 2010, ISSN: 1476-4687.

[10] J. J. Krauth *et al.*, "Measuring the α-particle charge radius with muonic helium-4 ions," *Nature*, vol. 589, no. 7843, pp. 527–531, 2021, ISSN: 1476-4687. DOI: 10.1038/s41586-021-03183-1.

[11] R. Pohl, R. Gilman, G. A. Miller, and K. Pachucki, "Muonic hydrogen and the proton radius puzzle," *Annual Review of Nuclear and Particle Science*, vol. 63, no. 1, pp. 175–204, 2013, ISSN: 0163-8998. DOI: 10.1146/annurev-nucl-102212-170627.

[12] V. Patkó, V. A. Yerokhin, and K. Pachucki, "Complete $\alpha^7 m$ lamb shift of helium triplet states," *Phys. Rev. A*, vol. 103, p. 042 809, 4 Apr. 2021. DOI: 10.1103/PhysRevA.103.042809. https://link.aps.org/doi/10.1103/PhysRevA.103.042809

[13] A. Cichocki *et al.*, "Electron scattering from ^{10}B," *Phys. Rev. C*, vol. 51, pp. 2406–2426, 5 May 1995. DOI: 10.1103/PhysRevC.51.2406. https://link.aps.org/doi/10.1103/PhysRevC.51.2406

[14] B. Maaß *et al.*, "Towards laser spectroscopy of the proton-halo candidate boron-8," *Hyperfine Interactions*, vol. 238, no. 1, p. 25, 2017, ISSN: 1572-9540. DOI: 10.1007/s10751-017-1399-5.

[15] B. Maaß *et al.*, "Nuclear charge radii of ^{10,11}B," *Phys. Rev. Lett.*, vol. 122, p. 182 501, 18 May 2019. DOI: 10.1103/PhysRevLett.122.182501. https://link.aps.org/doi/10.1103/PhysRevLett.122.182501

[16] W. Ruckstuhl *et al.*, "Precision measurement of the 2p-1s transition in muonic 12c: Search for new muon-nucleon interactions or accurate determination of the rms nuclear charge radius," *Nuclear Physics A*, vol. 430, no. 3, pp. 685–712, 1984, ISSN: 0375-9474. DOI: https://doi.org/10.1016/0375-9474(84)90101-5. https://www.sciencedirect.com/science/article/pii/0375947484901015

[17] I. Sick, "Precise nuclear radii from electron scattering," *Physics Letters B*, vol. 116, no. 4, pp. 212–214, 1982, ISSN: 0370-2693. DOI: 10.1016/0370-2693(82)90327-6. https://www.sciencedirect.com/science/article/pii/0370269382903276

ISBN: 978-3-95450-239-4 ISSN: none doi: 10.18429/JACoW-EBIST2022-FR1WH03

[18] W. Nörtershäuser *et al.*, "Nuclear charge radii of ^{7,9,10}Be and the one-neutron halo nucleus ^{11}Be," *Phys. Rev. Lett.*, vol. 102, p. 062 503, 6 Feb. 2009. DOI: 10.1103/PhysRevLett.102.062503. https://link.aps.org/doi/10.1103/PhysRevLett.102.062503

[19] P. Imgram *et al.*, "Collinear laser spectroscopy at ion-trap accuracy: Transition frequencies and isotope shifts in the $6s\ ^2S_{1/2} \rightarrow 6p\ ^2P_{1/2,3/2}$ transitions in Ba^+," *Phys. Rev. A*, vol. 99, p. 012 511, 1 Jan. 2019. DOI: 10.1103/PhysRevA.99.012511. https://link.aps.org/doi/10.1103/PhysRevA.99.012511

[20] K. König, J. Krämer, P. Imgram, B. Maaß, W. Nörtershäuser, and T. Ratajczyk, "Transition frequencies and hyperfine structure in $^{113,115}In^+$: Application of a liquid-metal ion source for collinear laser spectroscopy," *Phys. Rev. A*, vol. 102, p. 042 802, 4 Oct. 2020. DOI: 10.1103/PhysRevA.102.042802. https://link.aps.org/doi/10.1103/PhysRevA.102.042802

[21] K. König *et al.*, "A new collinear apparatus for laser spectroscopy and applied science (coala)," *Review of Scientific Instruments*, vol. 91, no. 8, p. 081 301, 2020. DOI: 10.1063/5.0010903. https://doi.org/10.1063/5.0010903. https://doi.org/10.1063/5.0010903

[22] P. Müller, K. König, P. Imgram, J. Krämer, and W. Nörtershäuser, "Collinear laser spectroscopy of Ca^+: Solving the field-shift puzzle of the $4s^2S_{1/2} \rightarrow 4p^2P_{1/2,3/2}$ transitions," *Phys. Rev. Research*, vol. 2, p. 043 351, 4 Dec. 2020. DOI: 10.1103/PhysRevResearch.2.043351. https://link.aps.org/doi/10.1103/PhysRevResearch.2.043351

[23] B. Maaß *et al.*, *A 4π fluorescence detection region for collinear laser spectroscopy*, 2020. DOI: 10.48550/ARXIV.2007.02658. https://arxiv.org/abs/2007.02658

ISBN: 978-3-95450-239-4 ISSN: none doi: 10.18429/JACoW-EBIST2022-FR2WH03

CHARGE-EXCHANGE FACTOR IN EBIT SPECTRAL ANALYSIS*

Y. Yang†, E. Takacs, A. Hosier, Clemson University, Clemson, USA
Dipti, Yu. Ralchenko, P. Szypryt, G. O'Neil, A. Naing, J. N. Tan
National Institute of Standards and Technology, Gaithersburg, USA
A. C. Gall, A. Foster, R. Smith, N. Brickhouse
Center for Astrophysics, Harvard-Smithsonian, Cambridge, USA
D. Schultz, Northern Arizona University, Flagstaff,USA

Abstract

Detailed modeling of the plasma in an electron beam ion trap (EBIT) not only requires cross section data of electron impact ionization, excitation, and recombination, but also requires knowledge of operating conditions, such as electron beam energy, density, number of neutral atoms, and relative velocities. In the EBIT, charge exchange recombination from the neutral background has a significant effect on the ionization balance despite the relatively low density of neutral ions. However, it becomes the key issue in modeling because experimental conditions are not well-known, and the uncertainties for the charge exchange cross section are difficult to estimate. In this work, we introduced a single charge exchange factor that includes the necessary experimental parameters (neutral density, relative ion velocity) and charge exchange cross section. An experimental method for determining the charge exchange factor is discussed and applied to a collisional-radiative model NOMAD [1]. Comparison between measured and simulated spectra of highly charged Fe ions, produced at the NIST EBIT, show excellent agreement, demonstrating the usefulness of the method.

INTRODUCTION

Electron Beam Ion traps (EBITs) are small scale laboratory devices that create and trap highly charged ions for spectroscopic studies [2]. The combination of a highly controllable EBIT, with plasma modeling (e.g. [1], [3]), allows for the production of important atomic data such as wavelengths, relative line intensities, and cross sections [4–6], needed to benchmark, test, and improve plasma codes. However, modeling of the EBIT plasma requires an understanding of underlying atomic processes and a reliable knowledge of the charge state distribution.

The charge state balance between ions is determined by a set of rate equations that connects the number density of ions via charge changing interactions. These atomic processes decrease (recombination) or increase (ionization) the charge state of the ions through elementary collisional interactions with free electrons in the electron beam and with other ions or neutral atoms in the trap region. Double or multiple ionization and recombination may also occur, changing the ion charge by more than one in a single event. Conditions in the trap region determine the relative importance of these processes. For our application the rate equation (see e.g. [7, 8]) takes the form:

$$\frac{dN_i}{dt} = J_e(N_{i-1}\sigma^I_{i-1} - N_i\sigma^I_i + N_{i+1}\sigma^R_{i+1} - N_i\sigma^R_i) + N_{i+1}N_0\langle\sigma^{CX}v_r\rangle_{i+1} - N_iN_0\langle\sigma^{CX}v_r\rangle_i \quad (1)$$

Where only single charge changing processes are assumed, and neighboring charge states are connected with number densities of N_{i+1}, N_i, and N_{i-1}. In Eq. 1, $J_e = n_e v$ denotes the electron current density, σ^I and σ^R are the cross sections corresponding to the sum of different ionization processes including electron impact ionization (EI), excitation followed by autoionization (EA), and recombination processes (R), including radiative recombination (RR) and dielectronic recombination (DR). Charge exchange (CX) recombination occurs between ions and neutral atoms within the EBIT plasma and is a critical component of the charge state balance. As shown in the last two terms of the equation, the number density of neutral atoms, N_0, and the relative velocity of the ions and neutral atoms, v_r, are not easily measured or estimated, and the cross section, σ^{CX}, is difficult to calculate with high accuracy [9–12].

To this end, we will describe how we have combined these unknown factors into a free parameter, termed charge exchange factor, and discuss a technique utilizing measured line intensities and well known theoretical cross sections to determine this factor. Finally we will demonstrate the results of applying this factor by comparing measured and simulated spectra.

CHARGE EXCHANGE FACTOR

The intensity I of a measured spectral line, produced from charge state i, is proportional to the number of ions of that charge state, N_i (determined by the rate equation, Eq. 1). It also depends on the fraction P of these ions in the particular upper level of the atomic transition (upper level population fraction) and A the transition probability to the lower level. The unidirectional electron beam within the EBIT produces anisotropic and polarized emission [13, 14]. Therefore, transition dependent correction factors, like the angular distribution and polarization of the line are included in the term C_t. Detector specific factors, such as spectrometer transmission function, detector efficiency, and solid angle are included in C_d.

* Work supported by the NIST Grant Award Numbers 70NANB19H024, the NASA Grant Award Number 80NSSC18K0234, and the National Science Foundation Award Number 1806494.

† yy4@g.clemson.edu

ISBN: 978-3-95450-239-4 ISSN: none doi: 10.18429/JACoW-EBIST2022-FR2WH03

$$I = N_i P A C_t C_d \tag{2}$$

The population fraction P is generally determined by a complex scheme of excitation and cascade processes between energy levels of the ion or even those of neighboring charge states (e.g. via autoionization and recombination processes). Collisional radiative codes specialized for the non-Maxwellian electron energy distribution of the EBIT, such as the NOMAD package [1], have proven to be successful in handling such calculations. The atomic data that goes into the transition, excitation, and recombination rates can come from reliable atomic structure codes, such as the Flexible Atomic Code (FAC) [15] or GRASP2K [16].

Following from Eq. 2 the intensity ratio of two spectral lines can be calculated as:

$$\frac{I_1}{I_2} = \frac{N_1 P_1 A_1 C_{t1} C_{d1}}{N_2 P_2 A_2 C_{t2} C_{d2}} \tag{3}$$

Here N_1 and N_2 represent the number of ions in the charge states where lines 1 and 2 originate. If the two lines originate from the same charge state and are close in wavelength, detector related factors are similar, so that Eq. 3 simplifies to:

$$\frac{I_1^{'}}{I_2^{'}} = \frac{P_1}{P_2}\frac{A_1}{A_2}\frac{C_{t1}}{C_{t2}} \tag{4}$$

Equation 4 expresses that the ratio of the line intensities depends on the $\frac{P_1}{P_2}$ ratio of the upper level populations multiplied by the $\frac{A_1}{A_2}$ ratio of the transition probabilities corrected by $\frac{C_{t1}}{C_{t2}}$, the factor related to the anisotropic and polarized emission.

For nearby lines originating from different charge states Eq. 4 also includes the ratio of the number of ions from each charge state, $\frac{N_1}{N_2}$, which depends on the charge state balance in the EBIT.

$$\frac{I_1^{''}}{I_2^{''}} = \frac{N_1}{N_2}\frac{I_1^{'}}{I_2^{'}} \tag{5}$$

The charge state balance is determined by the ionization and recombination cross sections shown in Eq. 1., therefore one can express any of these quantities as a function of the others and an experimentally determined line intensity ratio on the left hand side of Eq. 4.

As previously discussed, the density of neutral atoms, the relative velocity between ions and neutral atoms, and the charge exchange cross section in the last two terms of Eq. 1 are difficult to establish. Even with a well designed neutral gas injection system that allows for the precise injection of atoms into the EBIT [17], the neutral density is difficult to determine and theoretical estimation of the charge exchange cross sections of highly charged ions have large uncertainties [9, 11]. In addition, the $J_e = n_e v$ electron current density is also a factor that carries similar problems. Given that the line intensity ratios, Eq. 5, also depend on these factors through Eq. 1, both charge state balance and line intensity ratio calculations are affected.

A solution for precisely determining multiple physical parameters simultaneously to simulate EBIT spectra is to find a combination of these physical quantities and reduce the number of parameters in the models. As we will show below $\frac{n_0 v_r}{n_e v}$, what we call the charge exchange factor, is a parameter that, once determined for a certain experimental condition, allows for the accurate modeling of experimental spectral line intensities.

In order to show this, let us express the charge exchange factor based on the relative intensities of spectral lines based on Eqs. 1. and 5.

$$\frac{n_0 v_r}{n_e v} = \frac{\sigma_i^R + \sigma_i^I - \frac{N_{i+1}}{N_i}\sigma_{i+1}^R - \frac{N_{i-1}}{N_i}\sigma_{i-1}^I}{\frac{N_{i+1}}{N_i}\sigma_{i+1}^{CX} - \sigma_i^{CX}} \tag{6}$$

Where we have assumed that: 1.) there are steady state conditions in the EBIT [7], therefore, the left hand side of Eq. 1. is zero, 2.) the v_r average relative velocity of neutral atoms with respect to the ions is the same for all charge states involved in Eq. 6. If we further assume that 3.) the excitation transition rates of the spectral lines that are used to experimentally determine the charge exchange factor are considerably larger than the radiative cascades rates that feed the upper levels of these transitions, the ratios of the number of ions in neighboring charge states can be expressed as

$$R_i^{i+1} \equiv \frac{N_{i+1}}{N_i} = \frac{I_{i+1}^1 \sigma_i^{E2}}{I_i^2 \sigma_{i+1}^{E1}} \tag{7}$$

Where σ_i^{E2} represents the excitation cross sections that feed the upper level of transition I_i^2 in charge state i and respectively the same for $i + 1$.

Calculating the charge exchange factor based on Eq. 6 requires experimentally measured line intensity ratios and theoretically calculated ionization and recombination cross sections. However, it simplifies when i represents the one-electron H-like charge state, because in this case R^{i+1} becomes zero and using the notation by Eq. 7, the charge exchange factor becomes:

$$\frac{n_0 v_r}{n_e v} = \frac{R_i^{i-1}\sigma_{i-1}^I - \sigma_i^R - \sigma_i^I}{\sigma_i^{CX}} \tag{8}$$

One can also express the line intensity ratio with a linear dependence on the charge exchange factor.

$$\frac{I_{He}^2}{I_H^1} = \left(\frac{n_0 v_r}{n_e v}\sigma_H^{CX} + \sigma_H^R + \sigma_H^I\right)\left(\frac{\sigma_{He}^{E2}}{\sigma_H^{E1}}\right)\left(\frac{1}{\sigma_{He}^I}\right) \tag{9}$$

Substituting this ratio into Eq. 6 one can express the ratio of a He-like and Li-like line $\frac{I_{He}^1}{I_{Li}^2}$ with theoretical cross sections and the intensity ratio of Eq. 9. Because of the form of Eq. 6 this ratio will have a quadratic dependence on the charge exchange factor. Due to the definition of the charge

ISBN: 978-3-95450-239-4 ISSN: none doi: 10.18429/JACoW-EBIST2022-FR2WH03

exchange factor it is a small number. Therefore, the quadratic terms are negligible with respect to linear terms, and the ratio of He-like and Li-like lines also have a linear dependence on the charge exchange factor. By the same argument one can show that the ratios of spectral lines in neighboring charge states have a linear dependence on the charge exchange factor. Therefore, by comparing experimentally and theoretically determined line intensity ratios, the charge exchange factor can be calculated.

In modeling EUV and x-ray spectra, our group has successfully used the simple relationship $\sigma^{CX} = q \times 10^{-15}\,\mathrm{cm}^2$ for the charge exchange cross section of highly charged ions of charge q [18]. In order to confirm the q dependence we have performed classical trajectory Monte Carlo (CTMC) simulations [18] to determine the charge exchange cross sections between few electron charge states of Fe and neutral N_2 molecules. These calculations have confirmed the general linear dependence of the cross section with the ion charge with a $1/1.4$ scaling factor with respect to the previous formula: $\sigma^{CX}_{CTMC} = \frac{q\times 10^{-15}\,\mathrm{cm}^2}{1.4}$.

Incorporating a model dependent scaling factor of f_s we can simplify Eq. 6.

$$\frac{n_0 v_r}{n_e v} f_s = \frac{\sigma_i^R + \sigma_i^I - R_i^{i+1}\sigma_{i+1}^R - R_i^{i-1}\sigma_{i-1}^I}{R_i^{i+1} q_{i+1} - q_i} \qquad (10)$$

The scaling factor f_s for our previously used cross section is $f_s = 10^{-15}$ while for the CTMC based cross section is $f_s = \frac{10^{-15}}{1.4}$. By incorporating f_s into the definition of the charge exchange factor we have achieved our goal of a single parameter representing individually uncertain physical quantities of the EBIT. The uncertainty of the charge exchange factor based on Eq. 8. is determined by the theoretical uncertainty of the calculated cross sections and the statistical uncertainties of measured transitions involved. This is generally much better than uncertainties of the individual physical quantities that charge exchange factor represent.

TEST CASE: FEW-ELECTRON FE SPECTRA

In order to test the validity of our approach we have taken high energy-resolution x-ray spectra of few-electron Fe at the EBIT facility at the National Institute of Standards and Technology (NIST). The spectra were recorded with a recently installed x-ray microcalorimeter, which is an array of 192 transition-edge sensors (TES) [19]. Modeling of the measured spectra was performed with the non-Maxwellian collisional-radiative code NOMAD [1] that incorporated the charged exchange factor determined from Eq. 8.

The simulated spectra generated by the non-Maxwellian collisional-radiative (CR) modeling code NOMAD [1] were compared with measurements to understand the charge-state balance and to aid in line identifications. The main sources of charge exchange factor uncertainties are the theoretical predictions for the cross sections. Because the beam energy (in the range of 9.11 keV to 17.80 keV) is much higher than the Li-like ionization threshold 2.045keV [20], we assume that the Li-like ionization cross section is approaching the photoionization cross section which can be calculated very accurately. Therefore, the ratio of the summation of 5 Li-like lines (see Table 1) to the He-like strong resonance transition $1s2p\ ^1P_1 - 1s^2\ ^1S_0$ which have a linear dependence on the charge exchange factor can be used to determine the charge exchange factor based on Eq. 8 by comparing theoretically and experimentally measured line intensity ratios. In our model, we varied the charge exchange factor $\frac{n_0 v_r}{n_e v}$ as

Table 1: Li-like Energies from Ref. [20]

E_{lines} (eV)	Transition	Ref.
1085.07440	$1s^2 2p\ ^2P_{\frac{3}{2}} - 1s^2 3s\ ^2S_{\frac{1}{2}}$	[21,22]
1101.04030	$1s^2 2p\ ^2P_{\frac{1}{2}} - 1s^2 3s\ ^2S_{\frac{1}{2}}$	[21,22]
1109.93510	$1s^2 2p\ ^2P_{\frac{3}{2}} - 1s^2 3d\ ^2D_{\frac{5}{2}}$	[21,23]
1162.69910	$1s^2 2s\ ^2S_{\frac{1}{2}} - 1s^2 3p\ ^2P_{\frac{1}{2}}$	[21,23,24]
1167.59900	$1s^2 2s\ ^2S_{\frac{1}{2}} - 1s^2 3p\ ^2P_{\frac{3}{2}}$	[21,23,24]

a free parameter and calculated line intensity ratio of Li-like lines to He-like until good agreement was found with the measured ratios. This was repeated at each electron beam energy.

Once determined, the charge exchange factor was used in the FAC/NOMAD model. As shown in Fig. 1, we compared the theoretical prediction with the experimental measurement. The space charge offset has been included. The dominant charge states are H-like and He-like. The good agreement verified our results. Intensity ratios of the different charge states can be reproduced from the simulation.

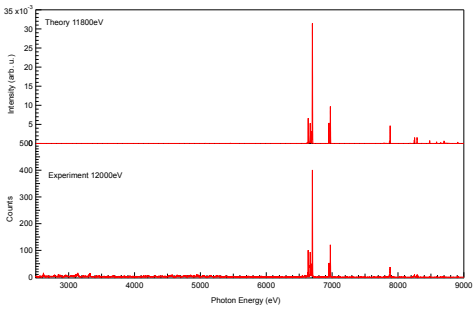

Figure 1: Comparison of measured spectra (E_b = 12.00 keV) and simulated spectra.

CONCLUSIONS

Plasma modeling is essential for the interpretation and extraction of atomic data from measured spectra. Understanding the charge state balance is a key part of modeling hot plasmas, but is a complex process due the difficulty in determining experimental parameters, such as the number of neutral atoms, or relative velocities. We have simplified this process by introducing a single unknown parameter,

ISBN: 978-3-95450-239-4 ISSN: none doi: 10.18429/JACoW-EBIST2022-FR2WH03

the charge exchange factor. We have tested our approach by analyzing x-ray spectra of highly charged Fe. We have determined the charge exchange factor at a number of electron beam energies and estimated the uncertainties, using a practical method of comparing measured and calculated line intensity ratios. When using the charge exchange factor in the detailed collisional-radiative model, we find excellent agreement between simulated and experimental spectra. This demonstrated our ability to model the EBITs plasma and will allow us to extract important atomic data, such as wavelengths and electron impact ionization cross sections from our measurements.

REFERENCES

[1] Y. V. Ralchenko and Y. Maron, "Accelerated recombination due to resonant deexcitation of metastable states,"*J. Quant. Spectrosc. Radiat. Transfer*, vol. 71, no. 2–6, pp. 609–621, Oct. 2001. doi:10.1016/s0022-4073(01)00102-9

[2] J. D. Gillaspy, "First results from the EBIT at NIST,"*Phys. Scr.*, vol. T71, pp. 99–103, Jan. 1997. doi:10.1088/0031-8949/1997/t71/017

[3] M. F. Gu, "The flexible atomic code,"*Can. J. Phys.*, vol. 86, no. 5, pp. 675–689, May 2008. doi:10.1139/p07-197

[4] K. L. Wong *et al.*, "Electron-impact ionization of lithiumlike ions: Ti^{19+}, V^{120+}, Cr^{21+}, Mn^{22+}, and Fe^{23+},"*Phys. Rev. A*, vol. 48, no. 5, pp. 2850-2859, Oct. 1993. doi:10.1103/PhysRevA.48.2850

[5] R. E. Marrs, S. R. Elliott, and D. A. Knapp, "Production and Trapping of Hydrogenlike and Bare Uranium Ions in an Electron Beam Ion Trap,"*Phys. Rev. Lett.*, vol. 72, no. 26, pp. 4082–4085, Jun. 1994. doi:10.1103/physrevlett.72.4082

[6] R. E. Marrs, S. R. Elliott, and J. H. Scofield, "Measurement of electron-impact ionization cross sections for hydrogenlike high-Z ions,"*Phys. Rev. A*, vol. 56, no. 2, pp. 1338–1345, Aug. 1997. doi:10.1103/physreva.56.1338

[7] F. Currell and G. Fussmann, "Physics of electron beam ion traps and sources,"*IEEE Trans. Plasma Sci.*, vol. 33, no. 6, pp. 1763–1777, Dec. 2005. doi:10.1109/tps.2005.860072

[8] B. M. Penetrante, J. N. Bardsley, D. DeWitt, M. Clark, and D. Schneider, "Evolution of ion-charge-state distributions in an electron-beam ion trap,"*Phys. Rev. A*, vol. 43, no. 9, pp. 4861–4872, May 1991. doi:10.1103/physreva.43.4861

[9] N. Selberg, C. Biedermann, and H. Cederquist, "Semiempirical scaling laws for electron capture at low energies,"*Phys. Rev. A*, vol. 54, no. 5, pp. 4127–4135, Nov. 1996. doi:10.1103/physreva.54.4127

[10] R. A. Phaneuf, "Electron capture by slow Fe^{q+} ions from hydrogen atoms and molecules,"*Phys. Rev. A*, vol. 28, no. 3, pp. 1310–1314, Sep. 1983. doi:10.1103/physreva.28.1310

[11] Y. F. Liu, K. Yao, R. Hutton, and Y. Zou, "Numerical simulations using an improved calculational scheme for ion charge state distribution and ion temperature evolution in an EBIT,"*J. Phys. B: At. Mol. Opt. Phys.*, vol. 38, no. 17, pp. 3207–3216, Aug. 2005. doi:10.1088/0953-4075/38/17/011

[12] Y. Ralchenko *et al.*, "EUV spectra of highly-charged ions W^{54+}–W^{63+} relevant to ITER diagnostics,"*J. Phys. B: At. Mol. Opt. Phys.*, vol. 41, no. 2, p. 021003, Jan. 2008. doi:10.1088/0953-4075/41/2/021003

[13] D. Savin, M. Gu, and P. Beiersdorfer, "The effects of electron spiraling on the anisotropy and polarization of photon emission from an electron beam ion trap,"in *Proc. The Japan-US Workshop on Plasma Polarization Spectroscopy and The International Seminar on Plasma Polarization Spectroscopy*, Kyoto, Japan, Jan. 1998, pp. 90–102.

[14] P. Beiersdorfer *et al.*, "Measurement and interpretation of the polarization of the x-ray line emission of heliumlike Fe XXV excited by an electron beam,"*Phys. Rev. A*, vol. 53, no. 6, pp. 3974–3981, Jun. 1996. doi:10.1103/physreva.53.3974

[15] M. F. Gu, "The Flexible Atomic Code,"*AIP Conf. Proc.*, vol 730, pp. 127–136, Oct. 2004. doi:10.1063/1.1824864.

[16] I. P. Grant, B. J. McKenzie, P. H. Norrington, D. F. Mayers, and N. C. Pyper, "GRASP: General-purpose Relativistic Atomic Structure Package,"Astrophysics Source Code Library, ascl:1609.008, https://ascl.net/1609.008

[17] K. Fahy *et al.*, "Extreme-ultraviolet spectroscopy of highly charged xenon ions created using an electron-beam ion trap,"*Phys. Rev. A*, vol. 75, no. 3, Mar. 2007. doi:10.1103/physreva.75.032520

[18] S. Otranto, R. E. Olson, and P. Beiersdorfer, "X-ray emission cross sections following charge exchange by multiply charged ions of astrophysical interest,"*Phys. Rev. A*, vol. 73, no. 2, Feb. 2006. doi:10.1103/physreva.73.022723

[19] P. Szypryt *et al.*, "A transition-edge sensor-based x-ray spectrometer for the study of highly charged ions at the National Institute of Standards and Technology electron beam ion trap,"*Rev. Sci. Instrum.*, vol. 90, no. 12, p. 123107, Dec. 2019. doi:10.1063/1.5116717

[20] A. Kramida, Yu. Ralchenko, J. Reader, and NIST ASD Team, NIST Atomic Spectra Database (ver. 5.9), https://physics.nist.gov/asd

[21] J. Reader, J. Sugar, N. Acquista, and R. Bahr, "Laser-produced and tokamak spectra of lithiumlike iron, Fe^{23+},"*J. Opt. Soc. Am. B*, vol. 11, no. 10, p. 1930, Oct. 1994. doi:10.1364/josab.11.001930

[22] M. A. Hayes, "Calculation of oscillator strengths and electron impact excitation collision strengths for Fe XXIV,"*Geophys. Suppl. Mon. Not. R. Astron. Soc.*, vol. 189, no. 1, pp. 55P-58P, Nov. 1979. doi:10.1093/mnras/189.1.55p

[23] L. Armstrong, W. R. Fielder, and D. L. Lin, "Relativistic effects on transition probabilities in the Li and Be isoelectronic sequences,"*Phys. Rev. A*, vol. 14, no. 3, pp. 1114–1128, Sep. 1976. doi:10.1103/physreva.14.1114

[24] Y.-K. Kim and J. P. Desclaux, "Relativistic f Values for the Resonance Transitions of Li- and Be-Like Ions,"*Phys. Rev. Lett.*, vol. 36, no. 3, pp. 139–141, Jan. 1976. doi:10.1103/physrevlett.36.139

ISBN: 978-3-95450-239-4 ISSN: none doi: 10.18429/JACoW-EBIST2022-FR3WH02

PROGRESS AND STATUS OF RAON EBIS CHARGE BREEDER*

Y.-H. Park†,[1], K.-H. Yoo[1,2], S. Heo[1], C. Lim[1,3], J. Lee[1], T. Shin[1], H.-J. Son[4], S. Kondrashev[5]
[1]Institute for Basic Science, Daejeon, Rep. of Korea
[2]Ulsan National Institute of Science and Technology, Ulsan, Rep. of Korea
[3]Korea University, Sejong, Rep. of Korea
[4]Facility for Rare Isotope Beams, Michigan State University, MI, USA
[5]Brookhaven National Laboratory, Upton, NY, USA

Abstract

An electron beam ion source (EBIS) was considered as a charge breeder for rare isotopes produced from isotope separation on-line (ISOL) system of the heavy ion accelerator RAON in Korea. The off-line installation of the RAON EBIS was conducted at the Korea University, Sejong from 2017 to 2020. A lot of effort went into getting very low vacuum pressure of around 10^{-10} Torr at the breeding region adopting cryopumps and getter pumps as well as vacuum-firing of the chambers. In order to find and align the central magnetic field lines of the solenoids, we used a gimbal mount for a hall probe with rotation, tilt, and translation functions. With the help of four sets of steering coils around the drift tube chamber, we successfully transport electron beam of 2 A atef a magnetic field of 6 T producing charge bred ions from the residual gas. After confirming the performance of our EBIS system at the off-line site, we moved it to RAON accelerator site at Shindong and started the on-line installation from 2021. Cesium test ion beam was used for the first charge breeding experiment showing a relative abundance of Cs^{27+} ions more than 20% with electron beam current of 1 A in breeding time of 40 ms.

INTRODUCTION

For the post-acceleration of the rare isotope beams, an electron beam ion source (EBIS) had been selected to be a charge breeder for RAON heavy ion accelerator in Korea [1-3]. Its design and development were accomplished by the help of experts from ANL, BNL, and CERN. The CARIBU-EBIS at ANL was the benchmark for the RAON EBIS [4-5] to meet the requirements of beam capacity and breeding efficiencies for various nuclear species. The electron gun and cathodes with maximum current of 3 A were purchased from the Budker Institute of Nuclear Physics. The Tesla Engineering Ltd won the contract of supplying the 6-T superconducting (SC) magnet which arrived at the off-line site, i.e., Korea University Sejong in 2017. Based on the electron beam transmission simulation, the collector was designed and manufactured. Most of the chambers and electrodes were produced by various Korean manufacturers. Parts were tested after their production and the whole system was assembled after confirming their performances. Figure 1 shows the off-line installation of RAON EBIS charge breeder at Korea University Sejong.

The test results of the electron gun and collector are described in the Ref. [6] in detail. Cryopumps, getter pumps, and turbo molecular pumps (TMPs) with high compression ratio were employed to maintain very low vacuum pressure around 10^{-10} Torr. Almost all chambers and stainless-steel structures inside vacuum were vacuum-fired to minimize the hydrogen outgassing. Vacuum test results are described in the Ref. [7] in detail. In the following sections, we describe the issues on magnetic field alignment, and the charge breeding results of the residual gas at the off-line site and cesium test ion beam at the on-line site.

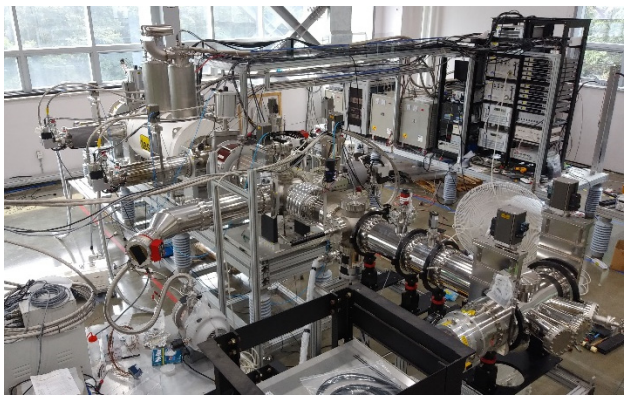

Figure 1: RAON EBIS charge breeder installed at Korea University Sejong.

ISSUES ON MAGNETIC FIELD

We considered making iron shields for TMPs and cryopumps because the ambient magnetic field from the SC magnet could cause the pumps to fail. A calculation of the magnetic field under asymmetric locations of the shields revealed that the magnetic line starting from the cathode ended around 10 mm away from the beam axis at the entrance of the collector. Therefore, we abandoned the plan for making the shields and decided to place the TMPs in a location where the surrounding field affects weaker to the TMPs. After placing the TMPs further from the SC magnet, where the magnetic line was parallel to the pump's rotation axis, we tested the robustness of the pump operation during the SC magnet was energized for several days. Only a TMP with magnetic bearing stopped with a roar when the SC magnet was ramping down, which we replaced with one with hybrid bearing afterwards.

* Work supported by the IBS/RISP funded by the Ministry of Science and ICT and the National Research Foundation of the Republic of Korea under Contract 2013M7A1A1075764
† yhpark@ibs.re.kr

ISBN: 978-3-95450-239-4 ISSN: none doi: 10.18429/JACoW-EBIST2022-FR3WH02

The inner structure of an ion gauge was bent along the magnetic line when the SC magnet was fully energized as shown in the inset of Fig. 2. Instead of making iron shields for the ion gauges, we measured the field direction at the gauge position and put elbowed nipples for the gauges to be aligned to the magnetic line as shown in Fig. 2. Without using the iron shields for ion gauges, we were able to turn on the gauges under a strong magnetic field although scaling of the pressure reading was necessary.

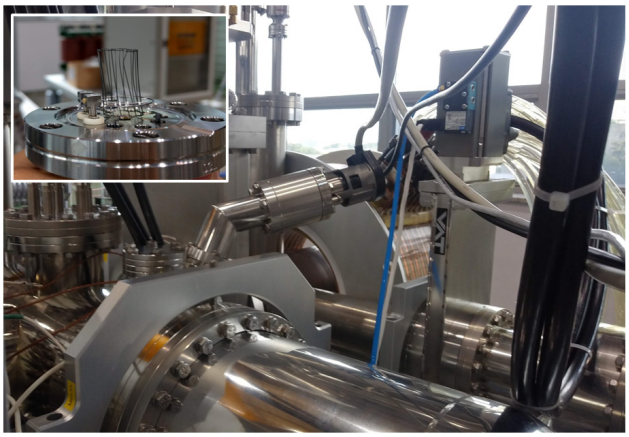

Figure 2: Ion gauge aligned to the magnetic line using the bent nipple. The inset shows the damaged inner structure of the ion gauge under a strong magnetic field.

Perfect alignment of magnetic line to the beam axis minimizes the loss of the electron beam transmitted from the cathode to the collector. To find the field center of the solenoids, we devised a gimbal mount as shown in Fig. 3. It has a rotatable circular disk with slots for attaching a hall probe at the center and the radially offset position. This disk can be tilted and shifted in horizontal and vertical directions. The procedure to find the field center of a solenoid using the gimbal mount is as follows. Radial components of the magnetic field against the rotation angles of the disk using a Hall probe at the center usually shows sinusoidal waveform giving information about whether the field direction is perpendicular to the disk plane or not. By adjusting the tilting knobs while minimizing the amplitude of the sinusoidal waveform, we can make the disk plane perpendicular to the magnetic field at the disk center.

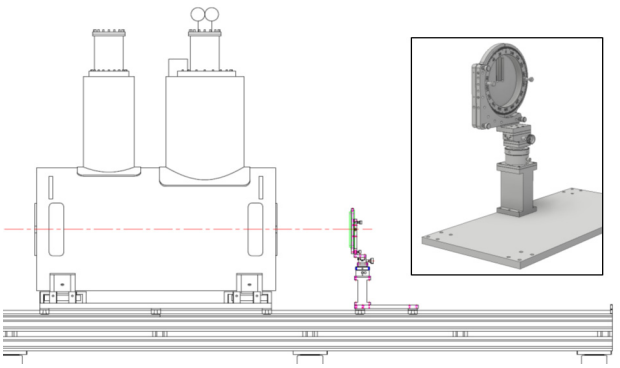

Figure 3: Gimbal mount to find the central magnetic line of solenoids.

Then we move the Hall probe to the radially offset position and measure the radial components of the magnetic field against the rotation angles again. Another sinusoidal waveform can be obtained and used to search for the field center by adjusting the shifting knobs. By iterating above procedures, we were able to mark the field center at both sides of the SC magnet. The offset of the field center from the mechanical bore center was found to be around 3 mm on the gun-side while, on the collector side, the offset was negligible.

The alignment of the whole EBIS system was performed with two identical alignment stages and a theodolite. The alignment stages with crosshair were positioned at the two ends of the EBIS stand as shown in Fig. 4. We located the theodolite several meters away from the EBIS stand so that the reticle of the theodolite's telescope overlapped with the crosshairs of the two alignment stages, which constituted the virtual beam axis. The flanges, the anode tube, the drift tubes, the entrance hole of the collector, SC magnet, gun coil, collector coil, etc. were positioned so that their centers lay on this virtual beam axis.

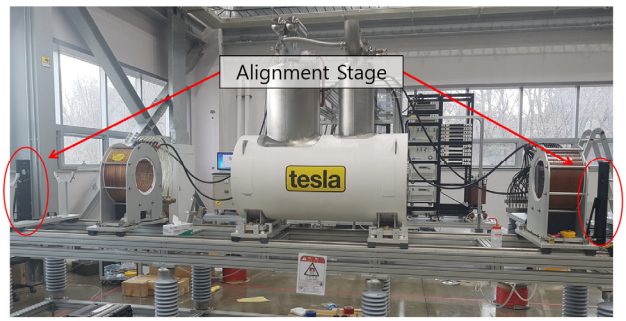

Figure 4: Alignment stages located at the two ends of the EBIS stand. The crosshairs of the stages constitute the virtual beam axis. We aligned every single element using this virtual line accessible through the telescope of the theodolite.

E-BEAM EXTRACTION

After several days of high voltage training for the assembled EBIS system, we started the electron beam extraction experiment. Four sets of steering coils as shown in Fig. 5 were used to minimize the loss of electron beam. We were able to obtain a 2-A electron beam with a pulse width of 50 ms and a repetition rate of 4 Hz. Afterwards we installed a dipole magnet at the end of the extraction beam line and obtained the very first charge breeding signal from the residual gas inside the chamber as shown in Fig. 6.

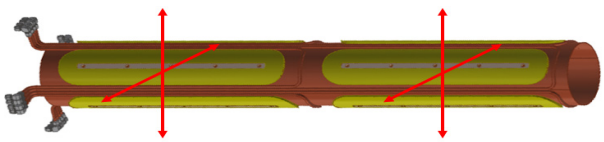

Figure 5: Four sets of Helmholtz-type steering coils wound on the water jacket for the drift tube chamber. The field-to-current ratio of a set of coils is 1.1 Gs/A.

ISBN: 978-3-95450-239-4 ISSN: none doi: 10.18429/JACoW-EBIST2022-FR3WH02

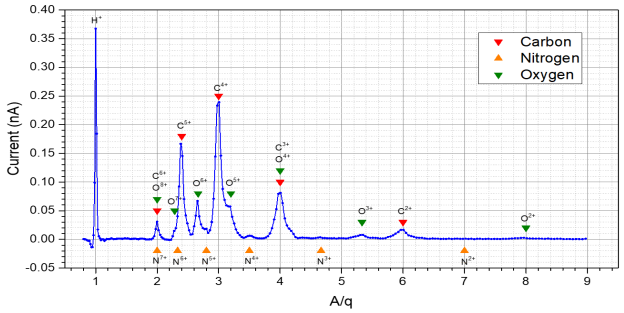

Figure 6: The very first charge breeding signal of the residual gas at the RAON EBIS charge breeder.

THE ON-LINE INSTALLATION

In October 2020, RAON EBIS was moved from Korea University Sejong to the ISOL low energy beamline at Shindong, Daejeon. The SC magnet, the drift tube chamber, the gun-side cross chamber, and the collector-side cross chamber were not taken apart, but kept assembled when moving on a vibration-free vehicle. Figure 7 shows the RAON EBIS system installed at the accelerator site. It took around 1 year for the whole system to be completely reassembled.

Figure 7: RAON EBIS charge breeder installed in the RAON ISOL beamline at Shindong site.

Figure 8 shows the first charge breeding signal of the Cs^{+} test ion after the installation at ISOL beamline. The relative abundance of Cs^{27+} ion was more than 20% with 1-A electron beam and breeding time of 40 ms. Based on Fig. 8, we were able to declare the completion of the development and installation of the RAON EBIS charge breeder.

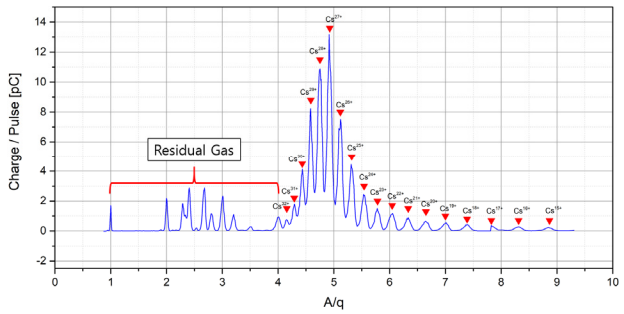

Figure 8: First charge breeding signal of Cs^{+} test ion.

Currently RAON EBIS routinely accepts bunched beams from the RFQ cooler buncher, charge-breeds ion beams of interest to required charge state, and sends them to the A/q separator to match the RFQ of the RAON injector system. Recently we performed pulse stretching experiment and obtained elongated pulse width of around 10 ms for end-user experiments requiring beams with much less intensity.

SUMMARY

At the final year of Rare Isotope Science Project, the RAON EBIS charge breeder was completely installed on RAON ISOL beamline and showed its design performances. The following table shows the system requirements of RAON EBIS charge breeder which have been fulfilled.

Table 1: System Requirements of RAON EBIS

Parameter	Value
Extraction beam energy	10 keV/u
A/q	< 6
Breeding time	50 ~ 100 ms
Capacity	Up to 10^8 ions / bunch
Repetition rate	~ 10 Hz
Beam pulse width	~ 100 μs

ACKNOWLEDGEMENT

While completing the RAON EBIS charge breeder, we have confronted several challenges like dealing with high voltages, strong magnetic field, ultrahigh vacuum, etc. Reviewers from other EBIS laboratories offered many valuable comments and recommendations during the developments, which guided us to finish this project successfully. We really appreciate their contributions.

REFERENCES

[1] T. Shin *et al.*, "Rare isotope production and experimental systems of RAON", *New Physics: Sae Mulli*, vol. 66, p. 1500, Dec. 2016. doi:10.3938/NPSM.66.1500

[2] S. Jeong *et al.*, "Progress of the RAON heavy ion accelerator project in Korea", in *Proc. 7th Int. Particle Accelerator Conf. (IPAC'16)*, Busan, Rep. of Korea, May 2016, pp. 4261-4265. doi:10.18429/JACoW-IPAC2016-FRYAA01

[3] H. J. Woo *et al.*, "Overview of the ISOL facility for the RISP", *J. Korean Phys. Soc.*, vol. 66, no. 3, p. 443, Feb. 2015. doi:10.3938/jkps.66.443

[4] H.-J. Son , Y.-H. Park, S. Kondrashev, J. Kim, B. J. Lee, and M. Chung, "Development of an EBIS charge breeder for the Rare Isotope Science Project", *Nucl. Instrum. Methods Phys. Res., Sect. B.*, vol. 408, p. 334, Mar. 2017. doi:10.1016/j.nimb.2017.03.131

[5] Y.-H. Park, H.-J. Son, and J. Kim, "Design of an EBIS Charge Breeder System for Rare-Isotope Beams", *J. Korean Phys. Soc.*, vol. 69, no. 6, p. 962, Sep. 2016. doi:10.3938/jkps.69.962

ISBN: 978-3-95450-239-4 ISSN: none doi: 10.18429/JACoW-EBIST2022-FR3WH02

[6] H.-J. Son, Y.-H. Park, T. Shin, S. Kondrashev, and M. Chung, "Electron gun and collector for RAON EBIS charge breeder", *J. Instrum.*, vol. 16, p. T09001, Sep. 2021. doi:10.1088/1748-0221/16/09/T09001

[7] H.-J. Son, Y.-H. Park, T. Shin, S. Kondrashev, and M. Chung, "Vacuum system for EBIS charge breeder of the RAON heavy ion accelerator", Vacuum, vol. 191, p. 110337, 2021. doi:10.1016/j.vacuum.2021.110337

ISBN: 978-3-95450-239-4 ISSN: none doi: 10.18429/JACoW-EBIST2022-FR3WH03

PolarX-EBIT – A VERSATILE TOOL FOR RESONANT X-RAY SPECTROSCOPY

R. Steinbrügge[†‡], Deutsches Elektronen-Synchroton DESY, 22607 Hamburg, Germany
S. Kühn, M. Togawa, J. R. Crespo-López Urrutia
Max-Planck-Institut für Kernphysik, 69117 Heidelberg, Germany
C. Shah, M. Leutenegger, NASA Goddard Space Flight Center, Greenbelt, MD 20771, USA
S. Bernitt, Helmholtz-Institut Jena, 07743 Jena, Germany

Abstract

Resonant photo-excitation provides a direct tool for investigating electronic transitions in atoms and ions. By combining EBITs and ultrabrilliant x-ray sources this kind of spectroscopy became also available for highly charged ions. Here we present the PolarX-EBIT, a compact permanent-magnet EBIT built by the Max Planck Institute for Nuclear Physics and University Jena specifically for operation at synchrotron radiation light source facilities. It employs a novel off-axis electron gun, allowing the photon beam to pass through the trap and be made available for downstream setups. Additionally, it features fast-switching power supplies for charge breeding and background reduction schemes, a time-of-flight ion extraction beamline and large area SDD detectors. Multiple successful experiments have been performed in the soft and hard x-ray regimes at the light sources BESSY II and PETRA III, measuring transition energies, oscillator strengths, natural line widths, photoionization and population balance. Furthermore, narrow lines of He-like ions have also been used as a diagnostic tool for the spectral performance of the photon beamlines.

INTRODUCTION

Electronic transitions in highly charged ions are of great importance for astronomy and astrophysics, as most matter in the universe is in an ionized form. Observed in x rays, their transitions are often the only spectroscopic features. Furthermore the strong electric field involved makes transitions in highly charged ions much more sensitive to relativistic and QED effects. Consequently, extensive spectroscopy measurements have been performed in EBITs and other plasma sources using electron impact as excitation mechanism.

As shown with laser spectroscopy in the optical region, more precise measurements can be performed when the excitation is induced by a photon. This resonant process allows selective excitation of states and thus more control over the atomic system.

Resonant Spectroscopy

By overlapping an ion cloud with a monochromatized photon beam, electronic transitions in highly charged ions can be selectively excited. The subsequent radiative decay of the excited state is observed by x-ray detectors mounted perpendicular to the photon beam. Spectra are recorded by scanning the incoming photon beam energy. The spectral resolving power is determined by the monochromator and other elements of the beamline. With the brightness of current generation synchrotron radiation sources, measurement times can be significantly reduced compared to conventional grating spectrometers.

This principle was developed and successfully applied during multiple campaigns with the FLASH-EBIT of the Max Planck Institute for Nuclear Physics [1–5].

PolarX-EBIT

Based on these campaigns with the FLASH-EBIT an EBIT permanently installed at a synchrotron radiation source was proposed and funded by a BMBF project, named PolarX-EBIT. In a joint development with the PTB-EBIT, a new type of compact permanent-magnet EBITs was designed and built. The main parameters of these EBITs are described in [6]. The modifications made for operation as part of an x-ray beamline are described in the following.

Off-axis Gun

To facilitate a permanent installation at a synchrotron radiation beamline, it is essential that the EBIT does not block the beam, so that other experiments can be performed when the EBIT is not in use or simultaneously to an EBIT measurement. For this reason an off-axis electron gun was designed, leaving the central axis of the EBIT free to pass the x-ray beam through the apparatus. The cathode is mounted below the axis under a 22° angle (see. Fig. 1). To bend the electron beam back onto the axis the anode and focus electrodes are split in two parts each. This design is more susceptible to the applied voltages, but with careful tuning beam transmission rates larger than 95% and electron currents up to 30 mA can be obtained.

X-ray Detectors

The PolarX-EBIT can be equipped with two large area (80 mm^2 and 150 mm^2) silicon drift detectors. The design of the trap allows to mount the detectors close to the trap, so that they cover a large solid angle up to 1 sr. 500 nm thick aluminum foil is mounted in front of them to block visible and VUV light. The detectors are mounted perpendicular to the photon beam and to each other. The two orientations allow investigation of the angular distribution of the emitted

† rene.steinbruegge@med.uni-heidelberg.de
‡ now at Heidelberg Ion Beam Therapy Center, 69120 Heidelberg, Germany

ISBN: 978-3-95450-239-4 ISSN: none doi: 10.18429/JACoW-EBIST2022-FR3WH03

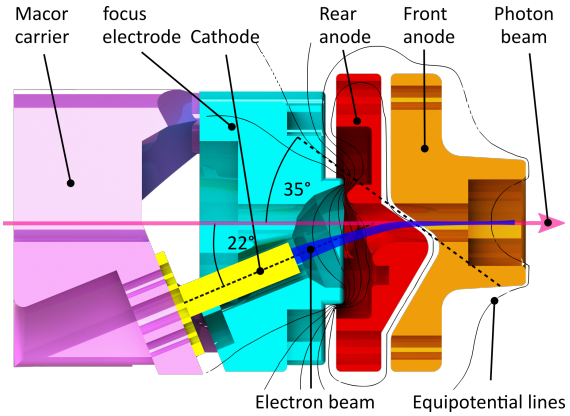

Figure 1: Layout of the off-axis gun. Figure taken from [6].

photons, which could be non-uniform if the ions are excited with polarized light.

Positioning System

The aperture of the gun and collector are just 4 mm in diameter, so precise alignment of the EBIT to the photon beam is important. This is achieved by a support frame with three feet, one front foot under the gun and two in the back, left and right of the collector. Each foot has a lifting spindle and is mounted on a translation stage, so the horizontal and vertical position, as well as pitch and yaw can be adjusted. All motions are motorized to allow remote control in radiation protected areas.

Electron Beam Energy Switching

For some measurements the electron-beam energy required to sufficiently produce the ion of interest is equal or larger than the transition energy probed. In this case the background created by electron impact excitation and radiative recombination overlaps the fluorescence signal, reducing the signal-to-noise ratio drastically. To circumvent this, an electron beam energy switching technique was implemented. The ions are charge bred at a high electron-beam energy, then the potentials of the trap electrodes are ramped down to a value causing no significant background. To avoid ion losses, ramping is performed with a sigmoidal shape while the trap depth is kept constant. At the low energy, the measurement can be performed. After a probing period, the energy is ramped up and the cycle starts again. Typical breeding and probing times are 0.1–1 s while the switching time is in the order of 10 ms.

Ion Extraction

To analyze the charge state distribution of the trapped ions, the PolarX-EBIT was equipped with a time-of-flight extraction beamline (see Fig. 2). It consists of an electrostatic 90° bender, a focusing lens and a channeltron detector. To extract the ions, the central trap electrode is instantaneously raised to 2 keV by a Behlke switch. By this the ions are kicked out of the trap and travel through the collector and the bender onto the channeltron, where the time-of-flight spectrum is acquired. From the time-of-flight, the charge-to-mass ratio can be determined. By observing changes in the charge state distribution, photoionization processes can be detected.

EXPERIMENTS

Since finishing construction in 2016 the PolarX-EBIT was successfully utilized for various measurement campaigns at different synchrotron radiation sources. During these experiments a lot of experience was gained. The installation and alignment of the EBIT can now be achieved within one day. Only a brief overview of the experiments can be given here, which are described in more detail in the referenced publications.

BESSY II

At the BESSY II beamline U49/2-PGM1 a gas cell was mounted behind the EBIT to simultaneously measure transitions of highly charged ions in the trap and O_2 photoionization. Using the K_δ, K_ϵ and K_ζ transitions in He-like N^{5+} to calibrate the photon beam energy, it was found that previous literature values of O_2 transitions were off by 450 meV [8]. Further gases were measured, proving the potential of highly charged ions as a reliable calibration source [9].

P04

Several beamtimes were performed at the soft x-ray beamline P04 of the PETRA III synchrotron radiation source at DESY. With its high photon flux and energy resolution it is ideally suited for resonance spectroscopy.

After initial measurements of the 3C/3D intensity ratio in neon-like iron [10], the signal-to-noise ratio could be greatly improved by the electron beam energy switching technique. Thus it was possible to measure the Lorentzian wings of those transitions. These accurate measurements for the first time yielded an intensity ratio in agreement with calculations. Furthermore, the natural linewidths of those lines could also be determined [11].

The extraction beamline was used to measure photoionization of Fe^{13+}, which was detected by the resulting Fe^{14+} photoions showing up in the time-of-flight spectra. Many transitions of the so-called unresolved transition array between 760 eV and 810 eV could be observed [7]. In addition to the Auger process, the radiative decay of the excited states was observed with the SDD detector which enables deductions about branching ratios.

As many lines of highly charged ions are much narrower than the ones usually found in neutral gases, they also provide a more precise diagnostic of the spectral line shape of the photon beam. Thus the strong *w* transitions of oxygen and neon were used to tune the P04 beamline [12].

P01

At the hard x-ray beamline P01 of PETRA III several beamtimes have been conducted with photon energies in the 6-15 keV range, investigating iron and krypton ions. As the charge states get higher, it becomes harder to produce

ISBN: 978-3-95450-239-4 ISSN: none doi: 10.18429/JACoW-EBIST2022-FR3WH03

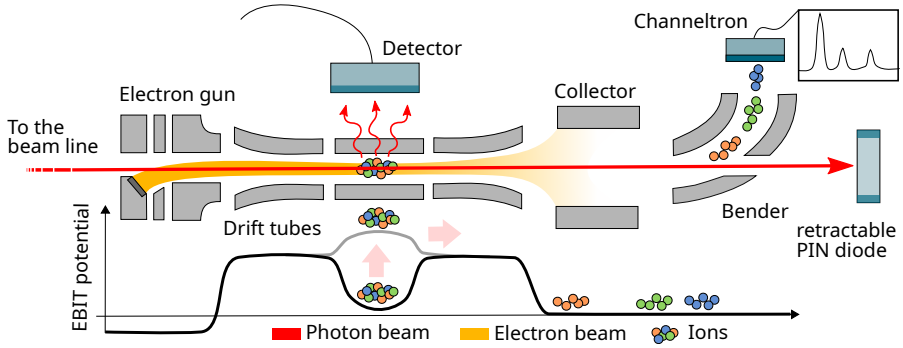

Figure 2: Scheme of the PolarX extraction principle. Figure taken from [7].

them with the electron beam current achievable with the off-axis gun. However, it was possible to measure K_α and K_β transitions in iron up to He-like Fe^{24+}. The high flux and resolving power of the P01 dual crystal monochromator allowed to measure transitions originating from metastable states in Fe^{22+} and Fe^{20+} [13]. Furthermore K_β transitions have been measured for several L-shell iron and krypton ions. For the latter the ^{57}Fe Mössbauer line at 14 412.497 eV was observed in parallel and used as a photon energy calibration reference.

CONCLUSION

The PolarX-EBIT has been successfully commissioned and used at various beamlines. The off-axis design has proven to be able to produce sufficient amounts of highly charged ions for resonance spectroscopy. It is a valuable addition to the experimental setup, allowing complementary measurements with the photon beam. With the charge-breeding scheme and ion extraction the range of addressable transitions could be extended. Furthermore the position and shape of transitions in highly charged ions have also been used as a diagnostic tool to improve the resolving power of the soft x-ray beamlines.

Following these pioneering works enabled by PolarX-EBIT, similar devices are currently under construction for the use at European XFEL, PAL-FEL, and Spring8.

ACKNOWLEDGEMENTS

Financial support was provided by the Max-Planck-Gesellschaft (MPG) and Bundesministerium für Bildung und Forschung (BMBF) through project 05K13SJ2. C.S. acknowledges the support by an appointment to the NASA Postdoctoral Program at the NASA Goddard Space Flight Center, administered by Oak Ridge Associated Universities under contract with NASA. M.A.L. acknowledges support from NASA's Astrophysics Program.

REFERENCES

[1] S. W. Epp *et al.*, "Soft X-Ray Laser Spectroscopy on Trapped Highly Charged Ions at FLASH," *Phys. Rev. Lett.*, vol. 98, p. 183 001, 18 May 2007. DOI: 10.1103/PhysRevLett.98.183001.

[2] M. C. Simon *et al.*, "Resonant and Near-Threshold Photoionization Cross Sections of Fe^{14+}," *Phys. Rev. Lett.*, vol. 105, no. 18, 183001, p. 183 001, Oct. 2010. DOI: 10.1103/PhysRevLett.105.183001.

[3] S. Bernitt *et al.*, "An unexpectedly low oscillator strength as the origin of the Fe XVII emission problem," *Nature*, vol. 492, no. 7428, pp. 225–228, Dec. 2012, ISSN: 1476-4687. DOI: 10.1038/nature11627.

[4] J. K. Rudolph *et al.*, "X-ray resonant photoexcitation: Linewidths and energies of $K\alpha$ transitions in highly charged fe ions," *Phys. Rev. Lett.*, vol. 111, p. 103 002, 10 Sep. 2013. DOI: 10.1103/PhysRevLett.111.103002.

[5] R. Steinbrügge *et al.*, "Absolute measurement of radiative and auger rates of $K-$shell$-$vacancy states in highly charged fe ions," *Phys. Rev. A*, vol. 91, p. 032 502, 3 Mar. 2015. DOI: 10.1103/PhysRevA.91.032502.

[6] P. Micke *et al.*, "The Heidelberg compact electron beam ion traps," *Rev. Sci. Instrum.*, vol. 89, no. 6, p. 063 109, 2018. DOI: 10.1063/1.5026961.

[7] M. Togawa, "Investigation of the M-shell unresolved transition array of aluminium-like iron using monochromatic soft x-ray synchrotron radiation," M.S. thesis, Ruprecht-Karls-Universität, Heidelberg, 2021. http://hdl.handle.net/21.11116/0000-0009-1029-7

[8] M. Leutenegger *et al.*, "High-Precision Determination of Oxygen K_α Transition Energy Excludes Incongruent Motion of Interstellar Oxygen," *Phys. Rev. Lett.*, vol. 125, p. 243 001, 24 2020. DOI: 10.1103/PhysRevLett.125.243001.

[9] J. Stierhof *et al.*, "A new benchmark of soft x-ray transition energies of Ne, CO_2, and SF_6: Paving a pathway towards ppm accuracy," *The European Physical Journal D*, vol. 76, no. 3, p. 38, Mar. 2022, ISSN: 1434-6079. DOI: 10.1140/epjd/s10053-022-00355-0.

[10] S. Kühn *et al.*, "High Resolution Photoexcitation Measurements Exacerbate the Long-Standing Fe XVII Oscillator Strength Problem," *Phys. Rev. Lett.*, vol. 124, p. 225 001, 22 Jun. 2020. DOI: 10.1103/PhysRevLett.124.225001.

[11] S. Kühn *et al.*, "Oscillator-strength ratio of two Fe XVII soft X-ray transitions essential for plasma diagnostics finally agrees with theory," 2022. https://arxiv.org/abs/2201.09070

[12] M. Hoesch *et al.*, "Highly Charged Ions for High-Resolution Soft X-ray Grating Monochromator Optimisation," in *presented at the 14th International Conference on Synchrotron Radiation Instrumentation (SRI), Hamburg, Germany*, 2022.

[13] R. Steinbrügge *et al.*, "X-ray Photoabsorption by Metastable Highly Charged Ions," *submitted for publication*, 2022.